Flow-Bench: A Dataset for Computational Workflow Anomaly Detection

George Papadimitriou[†][*]   **Hongwei Jin**[‡][*]   **Cong Wang**[§]   **Rajiv Mayani**[†]

Krishnan Raghavan[‡]   **Anirban Mandal**[§]   **Prasanna Balaprakash**[¶]   **Ewa Deelman**[†]

[†] University of Southern California
Los Angeles, CA
{georgpap,mayani,deelman}@isi.edu

[‡] Argonne National Laboratory
Lemont, IL
{jinh, kraghavan}@anl.gov

[§] RENCI
Chapel Hill, NC
{cwang, anirban}@renci.org

[¶] Oak Ridge National Laboratory
Oak Ridge, TN
pbalapra@ornl.gov

Abstract

A computational workflow, also known as workflow, consists of tasks that must be executed in a specific order to attain a specific goal. Often, in fields such as biology, chemistry, physics, and data science, among others, these workflows are complex and are executed in large-scale, distributed, and heterogeneous computing environments prone to failures and performance degradation. Therefore, anomaly detection for workflows is an important paradigm that aims to identify unexpected behavior or errors in workflow execution. This crucial task to improve the reliability of workflow executions can be further assisted by machine learning-based techniques. However, such application is limited, in large part, due to the lack of open datasets and benchmarking. To address this gap, we make the following contributions in this paper: (1) we systematically inject anomalies and collect raw execution logs from workflows executing on distributed infrastructures; (2) we summarize the statistics of new datasets, and provide insightful analyses; (3) we convert workflows into tabular, graph and text data, and benchmark with supervised and unsupervised anomaly detection techniques correspondingly. The presented dataset and benchmarks allow examining the effectiveness and efficiency of scientific computational workflows and identifying potential research opportunities for improvement and generalization. The dataset and benchmark code are publicly available `https://poseidon-workflows.github.io/FlowBench/` under the MIT License.

1 Introduction

Computational workflows that run on distributed and parallel computing environments, such as Southern California Earthquake Center's (SCEC) Cybershake [Callaghan et al., 2014] and LIGO's PyCBC [Nitz et al., 2024], have become an integral part of scientific, engineering, and data science research, enabling the simulation and modeling of complex otherwise impossible complex phenomena.

---

[*]Equal contribution.

Preprint. Under review.

However, in recent years, the scale and complexity of computational workflow systems have increased significantly. This increase has made these workflow applications prone to various types of hardware and software faults, including performance anomalies, crashes, and security breaches. These faults can cause significant disruptions to high-performance computing (HPC) applications, resulting in lost productivity, wasted resources, and potentially serious consequences for scientific discoveries.

To address this challenge, anomaly detection has emerged as a promising approach for detecting and diagnosing workflow failures. Anomaly detection refers to the process of identifying patterns or behaviors that deviate significantly from expected (or normal) behavior. Detection of anomalies enables system administrators and users to take proactive measures to prevent or mitigate the impact of faults, improving the overall reliability and efficiency of the workflow. Recently, various research efforts have been devoted to developing and evaluating anomaly detection techniques for computational workflows. While anomaly detection in workflows is very desirable, key challenges still persist: (1) there is no template for determining the relevance of deviations in the workflow settings, (2) most of the time, the training data is comprised of several orders of magnitude more data points corresponding to the normal than the anomaly, and (3) more often than not, labeling the anomalies in workflows incurs of lots of time and effort.

These fundamental challenges make the anomaly detection problem hard. Although standard anomaly detection benchmarks such as Zhao et al. [2019b] and Liu et al. [2022] can be applied to workflows. As is shown in this work, these methods are not very effective and do not scale well with the size of the workflow as well. Specifically, we show in Appendix I that many readily available anomaly detection methods result in out-of-memory (OOM) errors when encountering simple workflow data. On the other hand, the methods that do manage to work on the workflow data do not provide desirable precision. Moreover, there is still a lack of consensus on the best practices and benchmark datasets that facilitate the evaluation of different anomaly detection techniques on computational workflows, making it difficult to compare and reproduce the results of different studies.

These challenges indicate the need for careful analysis and study of workflow data, but the benchmarks needed for such analysis of workflows are not available in the literature. In this work, we present a set of novel workflows along with best practices and preliminary analysis that will provide the tools for future research to test and develop tools to facilitate anomaly detection on workflows. In particular, we present a benchmark study of anomaly detection techniques for workflows. We introduce a set of new workflow data that we have collected for anomaly detection and evaluate the performance of several state-of-the-art anomaly detection techniques, including tabular data anomaly detection [Zhao et al., 2019b], graph data anomaly detection [Liu et al., 2022, Kipf and Welling, 2017], and text data in supervise fine-tuned language models [Guo et al., 2021] in supervised and unsupervised way. Our evaluation is based on both supervised and unsupervised learning with several performance metrics, including accuracy, ROC-AUC score, F1-score, top-k score, etc. We compare the strengths and weaknesses of different anomaly detection techniques and reveal insights into their applicability and limitations in scientific workflow scenarios.

In spite of our benchmark being focused on computational workflows, it is important to note that challenges such as non-stationarity in input data distribution, differences in the number of nodes and features, the size of the data, and especially the lack of labels, provide a real-world example that can be readily utilized for the development of anomaly detection tools for the larger machine learning (ML) community. In contrast, popular benchmark tools such as PyOD [Zhao et al., 2019b] and PyGOD [Liu et al., 2022] do not provide these unique features.

1.1 Contributions

We introduce a set of workflow data that allows the careful study and development of novel anomaly detection approaches for computational workflows. We provide a comprehensive study to demonstrate the utility of our data with already available benchmarks and why novel methods are necessary.

2 Related Works

There are several techniques that have been proposed for anomaly detection. Statistical methods, machine learning (ML) methods, rule-based methods, and hybrid methods are the four major categories of these methods. Statistical methods formulate the anomaly detection problem as the detection of outliers in a distribution, and therefore, methods such as clustering [Sohn et al., 2023], principal

component analysis (PCA) [Ma et al., 2023], and auto-regressive integrated moving average (ARIMA) models [Goldstein, 2023] are commonly utilized. On the other hand, the ML methods involve learning a classifier map between the anomaly class and the input data. These methods have been developed for both tabular and graph data, and popular methods include (graph) neural networks [Yuan et al., 2021], decision trees [Breiman, 2001], and support vector machines (SVMs) [Schölkopf et al., 2001]. Hybrid methods take the probabilistic efficiency of statistical methods and combine it with the ability of ML methods to characterize complex distribution to improve the accuracy and robustness of anomaly detection [Kriegel et al., 2008]. Most recently, leveraging supervised fine-tuning and training large language models (LLMs) [Vaswani et al., 2017] on anomaly-labeled text data enables them to amplify their ability to detect unusual language patterns specific to the domain, making them highly effective for anomaly detection.

Another class of anomaly detection methods involves rule-based methods or expert systems where a set of rules must be defined to characterize normal system behavior. These rules can then be used to detect anomalies [Liu et al., 2008] in the data. These rules can either be based on expert knowledge or derived from historical data or ML or probabilistic models that encode normal information. While a non-exhaustive list of anomaly detection methods is presented above, all these methods can be potentially used in workflows. However, it is important to note that the choice of technique(s) for anomaly detection in workflows depends on the specific requirements and characteristics of the system being monitored, as well as the goals of the anomaly detection. For instance, a graph neural network (GNN)–based approach is more suitable for workflows than methods designed for tabular data because the dependency structure present in workflow data is rather important to characterize anomalies in computational workflows. Furthermore, computational workflows are unique in the setup as each workflow differs in the number of jobs, the dependency graph, and other structures. While training a separate anomaly detection approach for each workflow is inefficient, typical approaches discussed above, except the graph neural network-based, are unsuitable when the input data dimensions change for every computational workflow. On the other hand, workflow data can be rather large, and complex ML-based approaches run out of memory when trying to detect anomalies in these datasets.

In the past, datasets containing system logs of large systems (e.g., BlueGene, Thunderbird) have been released to the community Oliner and Stearley [2007]. However, these logs are unstructured, and they don't match the statistics and events to the workloads that were executed on these systems. Providing a dataset directly correlating system logs and the workflow application is important in creating new ML methods that better capture and identify workflow anomalies.

3 Dataset

The datasets used for benchmarking anomaly detection in computational workflows should represent the data types encountered in real applications. The datasets should include both normal and anomalous data to evaluate the performance of the base method. Some important statistics that should be considered when selecting datasets are:

- **Data size**: The dataset should be large enough to capture the variability in the data but not so large that it becomes computationally impractical to analyze and benchmark.

- **Data dimensionality**: The dataset's number of features or variables should represent the data types encountered in real applications.

- **Data distribution**: The dataset should represent the typical data distribution encountered in real applications.

3.1 Workflow Applications

Towards this end, we choose twelve workflow applications that are unique in their characteristics and are representative of real-world applications across multiple domains.

1000 Genome Workflow The 1000 genome project [1000 Genomes Project Consortium, 2012] provides a reference for human variation, having reconstructed the genomes of 2,504 individuals across 26 different populations. The test case we have here identifies mutational overlaps using data from the 1000 genomes project in order to provide a null distribution for rigorous statistical evaluation of potential disease-related mutations. This workflow (Figure 3 in Appendix B) is composed of five different tasks.

Montage Workflow   Montage is an astronomical image toolkit [Jacob et al., 2010] with components for re-projection, background matching, co-addition, and visualization of FITS files. Montage workflows typically follow a predictable structure based on the inputs, with each stage of the workflow often taking place in discrete levels separated by some synchronization/reduction tasks (mConcatFit and mBgModel). The workflow (Figure 4 in Appendix B) uses the Montage to transform astronomical images into custom mosaics, and is composed of eight different tasks.

Predict Future Sales (Data Science) Workflow   The predict future sales workflow [Kaggle, 2020] tackles Kaggle's predict future sales competition by receiving daily historical sales data from January 2013 to October 2015 and attempting to predict the sales for November 2015. It includes preprocessing, feature engineering, dataset segmentation based on type and sales performance, hyperparameter tuning, training of 3 XGBoost models for each group, and an ensemble technique to combine the model predictions into a single output file. Figure 5 in Appendix B illustrates the eleven-task workflow.

Variant Calling Workflow   The variant calling workflow contains all the steps to detect variations and identify changes in a DNA sequence compared to a reference genome. This workflow is adapted from the Data Carpentry Lesson - Data Wrangling and Processing for Genomics [Carpentry, 2023], that provides a pipeline to align population samples to the reference genome and detects the differences that exist. Variant calling is a very important process in bioinformatics that scientists have to perform. Figure 6 in Appendix B presents the workflow, which is composed of six different tasks.

CASA Workflows   The Collaborative Adaptive Sensing of the Atmosphere (CASA) [McLaughlin et al., 2009] has deployed a network of Doppler radars in the Dallas-Fort Worth (DFW) area, in order to improve observations, predictions and responses to hazardous weather events.
The *Wind Speed* workflow [Lyons et al., 2019] is one of CASA's production pipelines that ingests single radar base data from all of the radars in the network and creates a gridded product representing the maximum observed wind speeds in the area. The workflow identifies areas of severe wind and correlates them with the location of critical infrastructure, such as hospitals. In case critical infrastructure is impacted, the workflow dispatches email alerts to the impacted locations. The workflow (Figure 7 in Appendix B) calculates the maximum observed wind velocity across multiple minutes of radar data, and has five different tasks.
The *Nowcast* workflow [Lyons et al., 2019] computes short-term advection forecasts, by splitting gridded reflectivity radar data into 31 grids and computing reflectivity predictions over the next 30 minutes. Every minute new predictions need to be generated and Figure 8 in Appendix B presents a nowcast workflow that processes data across multiple minutes using three different tasks.

Soil Moisture Spatial Inference Engine Workflow   The soil moisture spatial inference engine (SOMOSPIE) workflow processes spatial environmental data to generate training and evaluation datasets and produces machine learning models that can predict the moisture of the soil in the future. SOMOSPIE is a modular workflow with multiple stages and Figure 9 in Appendix B presents the data preparation part of the workflow to produce the training and evaluation data sets. The workflow is consisted of eight different tasks.

PyCBC Workflows   PyCBC [Nitz et al., 2024] is a software package used to explore astrophysical sources of gravitational waves. It contains algorithms to analyze gravitational-wave data, detect coalescing compact binaries, and make bayesian inferences from gravitational-wave data collected by detectors (e.g., LIGO [Collaboration et al., 2015]).
The *PyCBC Inference* [Biwer et al., 2019] workflow performs parameter estimation on gravitational-wave signals using Bayesian inference methods to incorporate prior knowledge and quantify uncertainties in the parameter estimates. Figure 10 in Appendix B presents the workflow that's consisted of nine different tasks.
The *PyCBC Search* [Usman et al., 2016] workflow sifts through noisy detector data to identify gravitational waves. It's a complex workflow application that dynamically steers itself using at-runtime generated subworkflows with over fifty different tasks (Figure 11 in Appendix B).

EHT Workflows   The Event Horizon Telescope (EHT) workflows reproduce the first image of a black hole in the galaxy M87 and there are three image processing pipelines [Patel et al., 2022]. The *EHT Difmap* workflow performs image reconstruction by employing iterative convolution with difference mapping. Figure 12 in Appendix B shows the workflow with four different tasks. The *EHT Imaging* workflow performs image reconstruction using the regularized maximum likelihood (RML) approach. Figure 13 in Appendix B shows the workflow with two different tasks. The *EHT Smili* workflow uses the Sparse Modeling Imaging Library for Interferometry (SMILI)

to introduce pre-calibrated datasets and perform image reconstruction using the RML approach. Figure 14 in Appendix B shows the workflow with three different tasks.

3.2 Data Collection

To execute the workflows described above, manage their execution and collect events and statistics, we used the Pegasus Workflow Management System (WMS) [Deelman et al., 2015].

3.2.1 Workflow Model

In Pegasus, workflows are represented as Directed Acyclic Graphs (DAGs), where nodes represent jobs, and edges represent sequential dependencies and data dependencies between the jobs. A job can only be submitted when all its dependencies have been met. For a more formal definition, a workflow is described as a DAG $\mathcal{G} = (\mathcal{V}, \mathcal{E})$, where $\mathcal{V} = \{v_1, \cdots, v_n\}$ represents the set of n jobs and $\mathcal{E} \subseteq \mathcal{V}^2$ represents data dependencies between jobs. If $e_{ij} = (v_i, v_j) \in \mathcal{E}$, job v_i must complete its execution before v_j can start, i.e., a directed edge $v_i \rightarrow v_j$. We define $succ(v_i) = \{v_k \,|\, (v_i, v_k) \in \mathcal{E}\}$ (resp. $pred(v_i) = \{v_k \,|\, (v_k, v_i) \in \mathcal{E}\}$) to be the successors (resp. predecessors) of the job $v_i \in \mathcal{V}$. A job (v_i) of a Pegasus workflow can be classified into one of these three categories: (1) *Compute* jobs describe computational tasks; (2) *Transfer* jobs move data to and from an execution site/node; (3) *Auxiliary* jobs create working directories, clean up unused data or perform other Pegasus internal bookkeeping tasks.

Additionally, Pegasus collects provenance data and events during the execution of a workflow and associates them with the jobs that produced them. The Pegasus Panorama extensions [Deelman et al., 2017, SciTech, 2017, Papadimitriou et al., 2021] enhance the workflow DAG with features containing execution metrics and infrastructure statistics per job (v_i). These extensions enable the collection of execution traces of computational tasks, the collection of statistics of individual data transfers, the collection of infrastructure-related metrics, and all of them are stored in an Elasticsearch instance [ELK Stack, 2018].

3.2.2 Execution Infrastructure

To facilitate the workflow execution, we provisioned resources at the NSF Chameleon Cloud [Keahey et al., 2020] and the FABRIC testbed [Baldin et al., 2019] (Figure 2 in Appendix A). We provisioned 4 VMs (16 Cores and 32GB RAM) on FABRIC and 3 Cascade Lake bare-metal nodes (48 Cores and 192GB RAM) on Chameleon. In FABRIC 1 had the role of *submit node*, 1 had the role of *data node* and 2 were responsible for network QoS to the workers (StarLight location). In Chameleon all nodes were *Docker container executor nodes* [Docker Inc., 2022] located in the same region (University of Chicago - UC). The connectivity between the two testbeds/regions was established over a high-speed layer 2 VLAN (25 Gbps). On our *data node* we configured an Apache HTTP server, and on our *submit node* we installed and configured the Pegasus WMS [Deelman et al., 2015] binaries to manage the workflow execution, alongside with HTCondor [HTCondor, 2023] to manage the baremetal resources we provisioned. To create an HTCondor pool of resources, we spawned HTCondor's Executor containers on the Docker nodes, and in the case of the Predict Future Sales workflow we created 18 containers with 8 cores and 32GB RAM each, and in all other cases we created 20 containers with 4 cores and 16GB RAM each. For the Predict Future Sales workflow, we assigned more resources to each executor container to accommodate the hyper-parameter optimization phase, which leverages multiple cores and demands more memory. Core and RAM resources were mapped to the containers using Docker's runtime options (cpuset, memory). To deliver data to the executor containers, we used the *data node's* HTTP server, and we capped the download and upload speed to 1Gbps per HTCondor Executor container.

3.2.3 Synthetic Anomalies

To introduce synthetic anomalies, we used Docker's runtime options to limit and shape the performance of the spawned container executor nodes. Through the runtime options, we were able to configure the amount of CPU time an executor container is allotted and limit the average I/O each executor container can perform. These capabilities are supported via Linux's control groups version 2 [Kernel, 2015]. This approach offers sufficient isolation among the executors and allows us to obtain reproducible results from each type of experiment.

Table 1: Overall Dataset Statistics. We label the nodes as Normal, CPU K and HDD K.

Normal: No anomaly is introduced – normal conditions.

CPU K: M cores are advertised, but on some nodes, K cores are not allowed to be used. ($K = 2, 3, 4 \ M = 4, 8 \ and \ K < M$)

HDD K: On some executor nodes, the average write speed to the disk is capped at K MB/s and the read speed at ($2 \times K$) MB/s. ($K = 5, 10$)

| Workflow | DAG Information | | #DAG Executions | | | | | | #Total Nodes per Type | | | | | |
| | Nodes | Edges | Normal | CPU | | | HDD | | Normal | CPU | | | HDD | |
				2	3	4	5	10		2	3	4	5	10
1000 Genome	137	289	50	100	25	-	100	75	32261	5173	756	-	5392	4368
Montage	539	2838	51	46	80	-	67	76	137229	4094	11161	-	8947	11049
Predict Future Sales	165	581	100	88	88	88	88	88	72609	3361	3323	3193	3321	3293
Variant Calling	371	792	80	80	80	-	75	80	115588	8287	7222	-	7365	8083
CASA Wind Speed	162	342	150	200	200	-	200	160	116836	8793	8382	-	8305	5104
CASA Nowcast	2081	4029	101	80	78	-	79	83	685045	49960	46664	-	46104	48328
Soil Moisture	60	185	125	98	97	-	92	93	24408	1706	1428	-	1344	1414
PyCBC Inference	17	26	206	89	74	-	67	66	6970	549	326	-	388	301
PyCBC Search	368	1025	102	100	100	-	104	100	151004	9495	9039	-	8324	8346
EHT Difmap	33	59	142	93	88	-	89	89	13000	1059	737	-	877	860
EHT Imaging	12	18	212	76	74	-	70	69	4908	354	241	-	261	248
EHT Smili	16	26	148	87	84	-	90	93	6471	437	325	-	382	417

3.3 Dataset Description

Table 1 presents statistics of the executable workflow DAGs on the provisioned resources. Throughout the data harvesting phase, we maintained the DAGs of the workflows unchanged, and the DAG information presented in Table 1 reflects the number of nodes and edges of the final executable workflow DAGs submitted by Pegasus. The dataset contains 6352 workflow executions, under normal and 2 anomalous conditions, with different anomaly levels. By using the method of Section 3.2.3 to inject synthetic anomalies, the anomalies are introduced on a per DAG node level, and as a result, each DAG execution can have a different set of anomalous nodes, since HTCondor negotiates which worker will accept a job at submission time. The dataset contains 6 tags *normal*, *cpu_2*, *cpu_3*, *cpu_4*, *hdd_5* and *hdd_10*, that label the DAG nodes appropriately. Finally, the dataset provides the raw logs generated by Pegasus WMS and our experimental harness, and a parsed version, where we combined the raw logs into a single log file for each DAG execution. In the raw data we are offering (1) the workflows and the configurations used to execute them; (2) the original workflow submit directories of all DAG executions; (3) the workflow management system logs; (4) an experiment log file mapping the workflow DAG executions to the injected anomalies; (5) provenance data of each job, gathered by the WMS; (6) an Elasticsearch instance with all the captured workflow events, transfer events and resource utilization traces. Since we acquired the logs and metrics using an ephemeral private cloud instance, there is no sensitive information included in the dataset. The total size of the raw logs is over 200GB.

3.3.1 Parsed Data

To generate the parsed version of the dataset, we combined information coming from the executable DAGs, the experiment log containing the anomaly labels, Pegasus' logs, and the events hosted in Elasticsearch (Figure 15). During parsing, a CSV log file gets generated for every workflow DAG execution and is saved under the corresponding anomaly folder. The features present in the parsed data are listed in Table 4 in the appendix with their corresponding description, and the total size of the parsed data is 783MB. More specific to text data, we prepare sentences to describe the job given the feature and values in the template of

```
"FEAT1 is VAL1 FEAT2 is VAL2 ...
FEATn is VALn, LABEL"
```
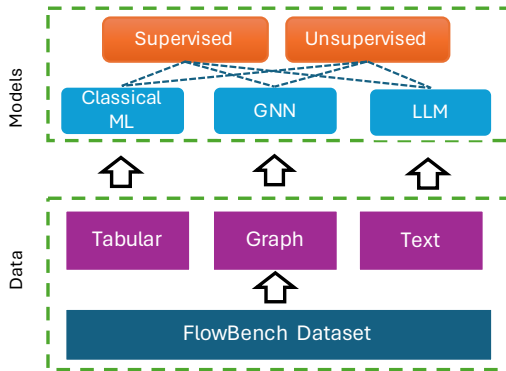

Figure 1: Overview of FlowBench

Table 2: Unsupervised Model Examples

Workflow	GAE (PyGOD)					GMM (PyOD)				
	Accuracy	AP	ROC-AUC	Recall@k	Train time(sec.)	Accuracy	AP	ROC-AUC	Recall@k	Train time(sec.)
1000 Genome	.664	.334	.523	.131	4.950	.660	.343	.525	.133	0.042
CASA Nowcast	.702	.213	.467	.048	39.390	.767	.259	.561	.195	0.529
CASA Wind Speed	.709	.202	.461	.039	8.978	.759	.227	.538	.160	0.085
EHT Difmap	.722	.214	.491	.085	2.204	.748	.226	.528	.145	0.031
EHT Imaging	.730	.175	.459	.036	1.728	.817	.267	.603	.265	0.020
EHT Smili	.710	.195	.446	.010	1.847	.761	.200	.504	.082	0.026
Montage	.715	.199	.466	.045	12.533	.753	.221	.529	.145	0.107
Predict Future Sales	.736	.183	.478	.063	6.725	.773	.200	.533	.153	0.053
PyCBC Inference	.762	.181	.508	.114	1.924	.781	.194	.537	.159	0.020
PyCBC Search	.722	.185	.457	.031	11.313	.759	.196	.516	.126	0.108
SOMOSPIE	.723	.191	.468	.047	3.168	.761	.204	.522	.130	0.033
Variant Calling	.722	.210	.490	.085	8.832	.763	.241	.549	.178	0.081

which can be used in the supervised fine-tuning of LLMs. All of our assets will be released under the MIT License.

4 ML Benchmarks on Computational Workflows

Anomaly detection in computational workflows is essential to ensure that experimental results are reliable and reproducible. A benchmark for anomaly detection in computational workflows would require selecting appropriate baseline methods and various metrics to evaluate the performance. We employ both the supervised and unsupervised approaches for the baselines due to the availability of labels in our scientific workflows. Table 5 in appendix D provides a set of selected algorithms with their details.

Supervised learning. Supervised anomaly detection models are trained on labeled data, where the job anomalies are already known. These models learn to identify anomalies based on the labeled data and can be used to detect anomalies in new, unlabeled data. Exampled classical methods are: support vector machine (SVM) [Hearst et al., 1998] , decision trees [Quinlan, 1986] , random forest [Breiman, 2001] , etc. Specific to the DAGs, there are (semi)supervised learning algorithms that can learn the structural and feature information simultaneously, such as GraphSAGE [Hamilton et al., 2017], GAT [Velivckovic et al., 2018], etc.

Unsupervised learning. Unsupervised anomaly detection models do not rely on labeled data and instead look for patterns or data points that are significantly different from the rest of the data. These methods are useful when it is difficult or impossible to obtain labeled data, which is typically the case in computational workflows. Exampled methods like: clustering (*e.g.*, k-means [Lloyd, 1982]) , density-based methods (*e.g.*, k-nearest neighbors [Ramaswamy et al., 2000]) , generative models (*e.g.*, auto-encoder [Sakurada and Yairi, 2014]) , etc. In this work, we adopt the methods from PyOD [Zhao et al., 2019b], where the data are considered as tabular data, and PyGOD [Liu et al., 2022], where the data are considered as structural data, as benchmarks, reporting a set of metrics, and provide insightful analysis of the data we collected.

Benchmarking setup. We began by converting our parsed data from Section 3.3.1 into a PyTorch Geometric (PyG) dataset [Fey and Lenssen, 2019], where each graph G is a DAG with nodes as jobs and edges as dependencies. PyG is widely used for graph data and can be converted to PyTorch and numpy tabular format for convenience in adapting existing models. We then normalized the datasets column-wise (feature) and aligned the timestamps. Finally, we randomly split the data into training, validation, and testing sets with a ratio of 7:1:2 with tabular, graph, and text data. A detailed data processing is provided in appendix E. The experiments were conducted on a single machine that featured two AMD EPYC 7532 processors, 256GB of local RAM, and an NVIDIA A100 GPU with a capacity of 40GB RAM. Because of the different backend implementations using either scikit-learn [Pedregosa et al., 2011] or PyTorch [Paszke et al., 2019], we give priority to using the GPU with the assistance of the CPU. More detailed hyperparameter setups of each algorithm are included in appendix F.

Metrics and benchmark results. Table 1 shows that the binary labels in the dataset are imbalanced. Therefore, performance is evaluated using metrics such as ROC-AUC, average precision, and top-k recall scores, in which we initially set the value of k to the number of true anomalies in the test set. In addition, we also provide the accuracy score for both supervised and unsupervised approaches for comparison across different methods.

Table 3: Supervised Model Examples

Workflow	GNN (GCN)					LLM-SFT (BERT-base-uncased)				
	Accuracy	AP	ROC-AUC	Recall@k	Train time(sec.)	Accuracy	AP	ROC-AUC	Recall@k	Train time(sec.)
1000 Genome	.794	.376	.555	.150	98.153	.776	.537	.746	.664	158.524
CASA Nowcast	.784	.217	.502	.007	2413.249	.796	.294	.584	.208	3215.485
CASA Wind Speed	.791	.210	.502	.005	264.580	.795	.233	.534	.090	515.584
EHT Difmap	.786	.215	.502	.006	27.223	.784	.282	.583	.231	54.185
EHT Imaging	.817	.190	.506	.014	11.002	.825	.175	.500	.000	19.759
EHT Smili	.805	.195	.500	.000	13.392	.840	.399	.657	.342	26.594
Montage	.795	.207	.502	.006	1092.069	.803	.240	.538	.091	572.677
Predict Future Sales	.814	.186	.500	.000	184.743	.861	.394	.667	.359	290.684
PyCBC Inference	.815	.185	.500	.000	15.316	.829	.222	.531	.066	27.950
PyCBC Search	.809	.191	.504	.014	421.313	.825	.255	.571	.166	610.556
SOMOSPIE	.801	.199	.500	.000	58.074	.809	.279	.606	.276	98.941
Variant Calling	.788	.214	.505	.014	275.890	.791	.252	.552	.139	483.320

The experimental evaluation encompassed the twelve novel scientific workflow applications introduced in this work, employing both supervised (Table 3) and unsupervised (Table 2) learning methodologies. The reported results constitute the mean values across five independent runs. Due to space constraints, comprehensive descriptions of the benchmarks, hyperparameter configurations, and complete results are provided in Appendix I. In Table 2, we present a comparative analysis of the Graph Auto-encoder (GAE) and Gaussian Mixture Model (GMM) architectures, which operate on graph and tabular data formats, respectively. It is noteworthy that the GAE approach exhibited significantly longer training times, despite leveraging GPU acceleration, without yielding substantial performance improvements over the established methods implemented in the PyOD library. The inefficiency observed in handling large-scale workflows can be attributed to the computational complexity associated with operations such as graph completion and reconstruction, which operate on sparse graph representations.

In Table 3, we present a comparative evaluation of supervised learning approaches, including Graph Convolutional Networks (GCN) and Supervised Fine-Tuned (SFT) models based on the BERT architecture with Low-Rank Adaptation (LoRA) [Hu et al., 2021] for parameter-efficient training, resulting in training with 0.72% of total parameters in BERT-base-uncased pre-trained model. The GCN models operate on graph-structured data, while the SFT models leverage textual inputs. It is observed that both methodologies necessitate substantial training efforts due to the inherent complexity of the underlying architectures. Notably, the SFT models based on pre-trained model, despite their relatively compact size, achieves superior performance on certain workflows (e.g., EHT Smili) compared to their GCN counterparts. The textual data, coupled with the knowledge distilled from large-scale pre-training corpora, enables the LLMs to capture not only the topological dependencies encoded in the graph representations but also the intricate system configurations present in the textual descriptions. This synergistic approach facilitates a more comprehensive understanding of the underlying job requirements within the scientific workflows.

Given the results from benchmarking methods, there is a clear need to develop novel methods to advance the state of the art and improve the performance of anomaly detection methods that scales to large-scale scientific workflows. The results also highlight the importance of developing methods that can handle the complexity and heterogeneity of computational workflows, as well as the need for more research in this area to improve the reliability and reproducibility of computational workflows.

5 Generalization and Limitations

In this work, we provide twelve workflows, eleven of which correspond to scientific applications and one of which corresponds to a data science workflow. While it is important to develop novel methods to facilitate unsupervised anomaly detection on these workflows, the use of these workflows in developing methods for a larger set of workflow anomaly detection problems is also relevant. Therefore, an important aspect of this work is the ability of the benchmark dataset to simulate anomalies across different scientific domains.

Since the workflow data is modeled as a DAG, it is feasible to use the ML methods that are developed to be precise on these workflows to work with other datasets that can be represented as DAG. Therefore, one may design approaches that can be built for anomaly detection for any application that generates data represented as a DAG, including workflows that are not represented in this benchmark since a wide range of anomalies can occur in real-world computational workflows.

Moreover, as we provide the raw log data, researchers can use it to explore new methods and approaches for anomaly detection beyond the ones presented in this work. This can lead to the development of more accurate and robust anomaly detection algorithms that can be applied to a wider range of computational workflows. For example, taking the context of the raw logs as inputs for natural language processing (NLP) tasks, such as large language models, can enable the development of more advanced anomaly detection algorithms that can capture the complex relationships between the various components of computational workflows, beyond the scope of graphs only capture the dependence between jobs.

Despite their usefulness, benchmark datasets with synthetic anomalies in computational workflows have some limitations. One limitation is that they may not fully capture the complexity and variability of real-world computational workflows. Scientific and data science workflows can be highly heterogeneous and may contain anomalies that are difficult to simulate using synthetic data. Another limitation is that benchmark datasets may not reflect the specific characteristics of the data in a particular scientific domain. Anomaly detection algorithms that perform well on benchmark datasets may not necessarily perform well on real-world data in a different scientific domain. Therefore, it is important to evaluate the performance of anomaly detection algorithms on real-world computational workflows in addition to benchmark datasets.

6 Conclusion

In this paper, we developed benchmark datasets for anomaly detection in computational workflows. Specifically, we have introduced a new dataset for benchmarking anomaly detection techniques, which includes systematically injected anomalies and raw execution logs from workflows executing on distributed infrastructures. We have also summarized the statistics of new datasets, including twelve computational workflows.

Our benchmarking, including both supervised and unsupervised approaches, provides effective methods for detecting anomalies in computational workflows. However, we also highlight the need for more research in this area, particularly in developing techniques that can handle the complexity and heterogeneity of computational workflows. We hope the study provides valuable insights into the challenges of anomaly detection in computational workflows and offers a starting point for future research in this area. We hope that our benchmark dataset and analysis will be useful for researchers and practitioners working on improving the reliability and reproducibility of computational workflows.

Acknowledgments and Disclosure of Funding

References

1000 Genomes Project Consortium. A global reference for human genetic variation. *Nature*, 526 (7571):68–74, 2012.

Samet Akcay, Amir Atapour-Abarghouei, and Toby P Breckon. Ganomaly: Semi-supervised anomaly detection via adversarial training. In *Computer Vision–ACCV 2018: 14th Asian Conference on Computer Vision, Perth, Australia, December 2–6, 2018, Revised Selected Papers, Part III 14*, pages 622–637. Springer, 2019.

Fabrizio Angiulli and Clara Pizzuti. Fast outlier detection in high dimensional spaces. In *Principles of Data Mining and Knowledge Discovery: 6th European Conference, PKDD 2002 Helsinki, Finland, August 19–23, 2002 Proceedings 6*, pages 15–27. Springer, 2002.

Andreas Arning, Rakesh Agrawal, and Prabhakar Raghavan. A linear method for deviation detection in large databases. In *Proceedings of the Second International Conference on Knowledge Discovery and Data Mining*, KDD'96, pages 164–169. AAAI Press, 1996.

Inc. Association of Universities for Research in Astronomy. Digitized sky survey, 1994. URL `https://catcopy.ipac.caltech.edu/dois/doi.php?id=10.26131/IRSA441`.

Ilya Baldin, Anita Nikolich, James Griffioen, Indermohan Inder S. Monga, Kuang-Ching Wang, Tom Lehman, and Paul Ruth. Fabric: A national-scale programmable experimental network infrastructure. *IEEE Internet Computing*, 23(6):38–47, 2019. doi: 10.1109/MIC.2019.2958545.

Tharindu R Bandaragoda, Kai Ming Ting, David Albrecht, Fei Tony Liu, Ye Zhu, and Jonathan R Wells. Isolation-based anomaly detection using nearest-neighbor ensembles. *Computational Intelligence*, 34(4):968–998, 2018.

Sambaran Bandyopadhyay, Saley Vishal Vivek, and MN Murty. Outlier resistant unsupervised deep architectures for attributed network embedding. In *Proceedings of the 13th international conference on web search and data mining*, pages 25–33, 2020.

C. M. Biwer, Collin D. Capano, Soumi De, Miriam Cabero, Duncan A. Brown, Alexander H. Nitz, and V. Raymond. Pycbc inference: A python-based parameter estimation toolkit for compact binary coalescence signals. *Publications of the Astronomical Society of the Pacific*, 131(996): 024503, jan 2019. doi: 10.1088/1538-3873/aaef0b. URL `https://dx.doi.org/10.1088/1538-3873/aaef0b`.

Johannes P. Blaschke, Aaron S. Brewster, Daniel W. Paley, Derek Mendez, Asmit Bhowmick, Nicholas K. Sauter, Wilko Kröger, Murali Shankar, Bjoern Enders, and Deborah Bard. Real-time xfel data analysis at slac and nersc: a trial run of nascent exascale experimental data analysis, 2021.

Leo Breiman. Random forests. *Machine learning*, 45:5–32, 2001.

Markus M Breunig, Hans-Peter Kriegel, Raymond T Ng, and Jörg Sander. Lof: identifying density-based local outliers. In *Proceedings of the 2000 ACM SIGMOD international conference on Management of data*, pages 93–104, 2000.

S. Callaghan, P. J. Maechling, G. Juve, K. Vahi, E. Deelman, and T. H. Jordan. Optimizing CyberShake Seismic Hazard Workflows for Large HPC Resources. In *AGU Fall Meeting Abstracts*, volume 2014, pages IN21C–3720, December 2014.

Data Carpentry. `https://datacarpentry.org/wrangling-genomics/index.html`, 2023.

Zhenxing Chen, Bo Liu, Meiqing Wang, Peng Dai, Jun Lv, and Liefeng Bo. Generative adversarial attributed network anomaly detection. In *Proceedings of the 29th ACM International Conference on Information & Knowledge Management*, pages 1989–1992, 2020.

Tainã Coleman, Henri Casanova, Loïc Pottier, Manav Kaushik, Ewa Deelman, and Rafael Ferreira da Silva. Wfcommons: A framework for enabling scientific workflow research and development. *Future Generation Computer Systems*, 128:16–27, 2022. doi: 10.1016/j.future.2021.09.043.

The LIGO Scientific Collaboration, J Aasi, and et al. Advanced ligo. *Classical and Quantum Gravity*, 32(7):074001, mar 2015. doi: 10.1088/0264-9381/32/7/074001. URL https://dx.doi.org/10.1088/0264-9381/32/7/074001.

Ewa Deelman, Karan Vahi, Gideon Juve, Mats Rynge, Scott Callaghan, Philip J Maechling, Rajiv Mayani, Weiwei Chen, Rafael Ferreira da Silva, Miron Livny, and Kent Wenger. Pegasus: a workflow management system for science automation. *Future Generation Computer Systems*, 46: 17–35, 2015. doi: 10.1016/j.future.2014.10.008.

Ewa Deelman, Christopher Carothers, Anirban Mandal, Brian Tierney, Jeffrey S Vetter, Ilya Baldin, Claris Castillo, Gideon Juve, Dariusz Król, Vickie Lynch, et al. Panorama: An approach to performance modeling and diagnosis of extreme-scale workflows. *The International Journal of High Performance Computing Applications*, 31(1):4–18, 2017.

Ewa Deelman, Karan Vahi, Mats Rynge, Rajiv Mayani, Rafael Ferreira da Silva, George Papadimitriou, and Miron Livny. The evolution of the pegasus workflow management software. *Computing in Science Engineering*, 21(4):22–36, 2019. doi: 10.1109/MCSE.2019.2919690.

Jacob Devlin, Ming-Wei Chang, Kenton Lee, and Kristina Toutanova. BERT: pre-training of deep bidirectional transformers for language understanding. *CoRR*, abs/1810.04805, 2018. URL http://arxiv.org/abs/1810.04805.

Kaize Ding, Jundong Li, Rohit Bhanushali, and Huan Liu. Deep anomaly detection on attributed networks. In *Proceedings of the 2019 SIAM International Conference on Data Mining*, pages 594–602. SIAM, 2019.

Docker Inc. Docker. https://docs.docker.com/, 2022.

ELK Stack, 2018. ELK stack. https://www.elastic.co/elk-stack, 2018.

Haoyi Fan, Fengbin Zhang, and Zuoyong Li. Anomalydae: Dual autoencoder for anomaly detection on attributed networks. In *ICASSP 2020-2020 IEEE International Conference on Acoustics, Speech and Signal Processing (ICASSP)*, pages 5685–5689. IEEE, 2020.

Rafael Ferreira da Silva, Rosa Filgueira, Ilia Pietri, Ming Jiang, Rizos Sakellariou, and Ewa Deelman. A characterization of workflow management systems for extreme-scale applications. *Future Generation Computer Systems*, 75:228–238, 2017. doi: 10.1016/j.future.2017.02.026.

Matthias Fey and Jan E. Lenssen. Fast graph representation learning with PyTorch Geometric. In *ICLR Workshop on Representation Learning on Graphs and Manifolds*, 2019.

Markus Goldstein. Special issue on unsupervised anomaly detection, 2023.

Markus Goldstein and Andreas Dengel. Histogram-based outlier score (hbos): A fast unsupervised anomaly detection algorithm. *KI-2012: poster and demo track*, 1:59–63, 2012.

Yury Gorishniy, Ivan Rubachev, Valentin Khrulkov, and Artem Babenko. Revisiting deep learning models for tabular data. *Advances in Neural Information Processing Systems*, 34:18932–18943, 2021.

Haixuan Guo, Shuhan Yuan, and Xintao Wu. Logbert: Log anomaly detection via bert. In *2021 international joint conference on neural networks (IJCNN)*, pages 1–8. IEEE, 2021.

William L Hamilton, Rex Ying, and Jure Leskovec. Inductive representation learning on large graphs. In *Proceedings of NIPS*, 2017.

Songqiao Han, Xiyang Hu, Hailiang Huang, Minqi Jiang, and Yue Zhao. Adbench: Anomaly detection benchmark. *Advances in Neural Information Processing Systems*, 35:32142–32159, 2022.

Johanna Hardin and David M Rocke. Outlier detection in the multiple cluster setting using the minimum covariance determinant estimator. *Computational Statistics & Data Analysis*, 44(4): 625–638, 2004.

Zengyou He, Xiaofei Xu, and Shengchun Deng. Discovering cluster-based local outliers. *Pattern recognition letters*, 24(9-10):1641–1650, 2003.

Marti A. Hearst, Susan T Dumais, Edgar Osuna, John Platt, and Bernhard Scholkopf. Support vector machines. *IEEE Intelligent Systems and their applications*, 13(4):18–28, 1998.

HTCondor, 2023. Htcondor, 2023.

Edward J Hu, Phillip Wallis, Zeyuan Allen-Zhu, Yuanzhi Li, Shean Wang, Lu Wang, Weizhu Chen, et al. Lora: Low-rank adaptation of large language models. In *International Conference on Learning Representations*, 2021.

Joseph C. Jacob, Daniel S. Katz, G. Bruce Berriman, John Good, Anastasia C. Laity, Ewa Deelman, Carl Kesselman, Gurmeet Singh, Mei-Hui Su, Thomas A. Prince, and Roy Williams. Montage: An Astronomical Image Mosaicking Toolkit. Astrophysics Source Code Library, record ascl:1010.036, October 2010.

Gideon Juve, Ann Chervenak, Ewa Deelman, Shishir Bharathi, Gaurang Mehta, and Karan Vahi. Characterizing and profiling scientific workflows. *Future Generation Computer Systems*, 29(3):682–692, March 2013. URL `http://pegasus.isi.edu/publications/2013/JuveG-Characterizing.pdf`.

Kaggle. `https://www.kaggle.com/c/competitive-data-science-predict-future-sales`, 2020.

Kate Keahey, Jason Anderson, Zhuo Zhen, Pierre Riteau, Paul Ruth, Dan Stanzione, Mert Cevik, Jacob Colleran, Haryadi S. Gunawi, Cody Hammock, Joe Mambretti, Alexander Barnes, François Halbach, Alex Rocha, and Joe Stubbs. Lessons learned from the chameleon testbed. In *Proceedings of the 2020 USENIX Annual Technical Conference (USENIX ATC '20)*. USENIX Association, July 2020.

Joseph P. Kenny, Jeremiah J. Wilke, Craig D. Ulmer, Gavin M. Baker, Samuel Knight, and Jerrold A. Friesen. An evaluation of ethernet performance for scientific workloads. In *2020 IEEE/ACM Innovating the Network for Data-Intensive Science (INDIS)*, pages 57–67, 2020. doi: 10.1109/INDIS51933.2020.00011.

Linux Kernel. `https://www.kernel.org/doc/html/latest/admin-guide/cgroup-v2.html`, 2015.

Thomas N Kipf and Max Welling. Variational graph auto-encoders. *arXiv preprint arXiv:1611.07308*, 2016.

Thomas N Kipf and Max Welling. Semi-supervised classification with graph convolutional networks. In *Proceedings of ICLR*, 2017.

Patrycja Krawczuk, George Papadimitriou, Ryan Tanaka, Tu Mai Anh Do, Srujana Subramany, Shubham Nagarkar, Aditi Jain, Kelsie Lam, Anirban Mandal, Loïc Pottier, and Ewa Deelman. A performance characterization of scientific machine learning workflows. In *2021 IEEE/ACM Workflows in Support of Large-Scale Science (WORKS)*, pages 58–65, 2021. doi: 10.1109/WORKS54523.2021.00013.

Hans-Peter Kriegel, Matthias Schubert, and Arthur Zimek. Angle-based outlier detection in high-dimensional data. In *Proceedings of the 14th ACM SIGKDD international conference on Knowledge discovery and data mining*, pages 444–452, 2008.

Longin Jan Latecki, Aleksandar Lazarevic, and Dragoljub Pokrajac. Outlier detection with kernel density functions. In *MLDM*, volume 7, pages 61–75, 2007.

Aleksandar Lazarevic and Vipin Kumar. Feature bagging for outlier detection. In *Proceedings of the eleventh ACM SIGKDD international conference on Knowledge discovery in data mining*, pages 157–166, 2005.

Jundong Li, Harsh Dani, Xia Hu, and Huan Liu. Radar: Residual analysis for anomaly detection in attributed networks. In *IJCAI*, volume 17, pages 2152–2158, 2017.

Fei Tony Liu, Kai Ming Ting, and Zhi-Hua Zhou. Isolation forest. In *2008 eighth ieee international conference on data mining*, pages 413–422. IEEE, 2008.

Kay Liu, Yingtong Dou, Yue Zhao, Xueying Ding, Xiyang Hu, Ruitong Zhang, Kaize Ding, Canyu Chen, Hao Peng, Kai Shu, Lichao Sun, Jundong Li, George H. Chen, Zhihao Jia, and Philip S. Yu. Bond: Benchmarking unsupervised outlier node detection on static attributed graphs. *Advances in Neural Information Processing Systems*, 35:27021–27035, 2022.

Stuart Lloyd. Least squares quantization in pcm. *IEEE transactions on information theory*, 28(2): 129–137, 1982.

Eric Lyons, George Papadimitriou, Cong Wang, Komal Thareja, Paul Ruth, J.J. Villalobos, Ivan Rodero, Ewa Deelman, Michael Zink, and Anirban Mandal. Toward a dynamic network-centric distributed cloud platform for scientific workflows: A case study for adaptive weather sensing. In *15th International Conference on eScience (eScience)*, pages 67–76, 2019. doi: 10.1109/eScience. 2019.00015. Funding Acknowledgments: NSF 1826997.

Zhi Ma, Yaozhi Luo, Chung-Bang Yun, Hua-Ping Wan, and Yanbin Shen. An mppca-based approach for anomaly detection of structures under multiple operational conditions and missing data. *Structural Health Monitoring*, 22(2):1069–1089, 2023.

David McLaughlin, David Pepyne, V. Chandrasekar, Brenda Philips, James Kurose, Michael Zink, Kelvin Droegemeier, Sandra Cruz-Pol, Francesc Junyent, Jerald Brotzge, David Westbrook, Nitin Bharadwaj, Yanting Wang, Eric Lyons, Kurt Hondl, Yuxiang Liu, Eric Knapp, Ming Xue, Anthony Hopf, Kevin Kloesel, Alfred DeFonzo, Pavlos Kollias, Keith Brewster, Robert Contreras, Brenda Dolan, Theodore Djaferis, Edin Insanic, Stephen Frasier, and Frederick Carr. Short-wavelength technology and the potential for distributed networks of small radar systems. *Bulletin of the American Meteorological Society*, 90(12):1797–1818, 2009. doi: 10.1175/2009BAMS2507.1. URL https://doi.org/10.1175/2009BAMS2507.1.

Ryan Mitchell, Loïc Pottier, Steve Jacobs, Rafael Ferreira da Silva, Mats Rynge, Karan Vahi, and Ewa Deelman. Exploration of workflow management systems emerging features from users perspectives. In *First International Workshop on Big Data Tools, Methods, and Use Cases for Innovative Scientific Discovery (BTSD)*, pages 4537–4544, 2019. doi: 10.1109/BigData47090.2019.9005494.

Alex Nitz, Ian Harry, Duncan Brown, Christopher M. Biwer, Josh Willis, Tito Dal Canton, Collin Capano, Thomas Dent, Larne Pekowsky, Gareth S Cabourn Davies, Soumi De, Miriam Cabero, Shichao Wu, Andrew R. Williamson, Bernd Machenschalk, Duncan Macleod, Francesco Pannarale, Prayush Kumar, Steven Reyes, dfinstad, Sumit Kumar, Márton Tápai, Leo Singer, Praveen Kumar, veronica villa, maxtrevor, Bhooshan Uday Varsha Gadre, Sebastian Khan, Stephen Fairhurst, and Arthur Tolley. gwastro/pycbc: v2.3.3 release of pycbc, January 2024. URL https://doi.org/10.5281/zenodo.10473621.

Adam J. Oliner and Jon Stearley. What supercomputers say: A study of five system logs. In *The 37th Annual IEEE/IFIP International Conference on Dependable Systems and Networks, DSN 2007, 25-28 June 2007, Edinburgh, UK, Proceedings*, pages 575–584. IEEE Computer Society, 2007. doi: 10.1109/DSN.2007.103. URL https://doi.org/10.1109/DSN.2007.103.

Guansong Pang, Chunhua Shen, and Anton van den Hengel. Deep anomaly detection with deviation networks. In *Proceedings of the 25th ACM SIGKDD international conference on knowledge discovery & data mining*, pages 353–362, 2019.

George Papadimitriou, Cong Wang, Karan Vahi, Rafael Ferreira da Silva, Anirban Mandal, Zhengchun Liu, Rajiv Mayani, Mats Rynge, Mariam Kiran, Vickie E Lynch, et al. End-to-end online performance data capture and analysis for scientific workflows. *Future Generation Computer Systems*, 117:387–400, 2021.

Adam Paszke, Sam Gross, Francisco Massa, Adam Lerer, James Bradbury, Gregory Chanan, Trevor Killeen, Zeming Lin, Natalia Gimelshein, Luca Antiga, et al. Pytorch: An imperative style, high-performance deep learning library. *Advances in neural information processing systems*, 32, 2019.

Ria Patel, Brandan Roachell, Silvina Caíno-Lores, Ross Ketron, Jacob Leonard, Nigel Tan, Karan Vahi, Duncan A. Brown, Ewa Deelman, and Michela Taufer. Reproducibility of the first image of a black hole in the galaxy m87 from the event horizon telescope collaboration. *Computing in Science & Engineering*, 24(5):42–52, 2022. doi: 10.1109/MCSE.2023.3241105.

F. Pedregosa, G. Varoquaux, A. Gramfort, V. Michel, B. Thirion, O. Grisel, M. Blondel, P. Prettenhofer, R. Weiss, V. Dubourg, J. Vanderplas, A. Passos, D. Cournapeau, M. Brucher, M. Perrot, and E. Duchesnay. Scikit-learn: Machine learning in Python. *Journal of Machine Learning Research*, 12:2825–2830, 2011.

Zhen Peng, Minnan Luo, Jundong Li, Huan Liu, Qinghua Zheng, et al. Anomalous: A joint modeling approach for anomaly detection on attributed networks. In *IJCAI*, pages 3513–3519, 2018.

James C. Phillips, David J. Hardy, Julio D. C. Maia, John E. Stone, João V. Ribeiro, Rafael C. Bernardi, Ronak Buch, Giacomo Fiorin, Jérôme Hénin, Wei Jiang, Ryan McGreevy, Marcelo C. R. Melo, Brian K. Radak, Robert D. Skeel, Abhishek Singharoy, Yi Wang, Benoît Roux, Aleksei Aksimentiev, Zaida Luthey-Schulten, Laxmikant V. Kalé, Klaus Schulten, Christophe Chipot, and Emad Tajkhorshid. Scalable molecular dynamics on CPU and GPU architectures with NAMD. *The Journal of Chemical Physics*, 153(4), July 2020. doi: 10.1063/5.0014475. URL https://doi.org/10.1063/5.0014475.

J. Ross Quinlan. Induction of decision trees. *Machine learning*, 1:81–106, 1986.

Sridhar Ramaswamy, Rajeev Rastogi, and Kyuseok Shim. Efficient algorithms for mining outliers from large data sets. In *Proceedings of the 2000 ACM SIGMOD international conference on Management of data*, pages 427–438, 2000.

Carl Rasmussen. The infinite gaussian mixture model. *Advances in neural information processing systems*, 12, 1999.

Dongwei Ren, Wangmeng Zuo, Qinghua Hu, Pengfei Zhu, and Deyu Meng. Progressive image deraining networks: A better and simpler baseline. In *Proceedings of the IEEE/CVF conference on computer vision and pattern recognition*, pages 3937–3946, 2019.

Lukas Ruff, Robert A Vandermeulen, Nico Görnitz, Alexander Binder, Emmanuel Müller, Klaus-Robert Müller, and Marius Kloft. Deep semi-supervised anomaly detection. In *International Conference on Learning Representations*, 2019.

David E Rumelhart, Geoffrey E Hinton, and Ronald J Williams. Learning representations by back-propagating errors. *Nature*, 323(6088):533, 1986.

Mayu Sakurada and Takehisa Yairi. Anomaly detection using autoencoders with nonlinear dimensionality reduction. In *Proceedings of the MLSDA 2014 2nd workshop on machine learning for sensory data analysis*, pages 4–11, 2014.

Bernhard Schölkopf, John C Platt, John Shawe-Taylor, Alex J Smola, and Robert C Williamson. Estimating the support of a high-dimensional distribution. *Neural computation*, 13(7):1443–1471, 2001.

SciTech, 2017. Pegasus panorama. https://github.com/pegasus-isi/pegasus/tree/panorama, 2017.

Mei-Ling Shyu, Shu-Ching Chen, Kanoksri Sarinnapakorn, and LiWu Chang. A novel anomaly detection scheme based on principal component classifier. Technical report, Miami Univ Coral Gables Fl Dept of Electrical and Computer Engineering, 2003.

Kihyuk Sohn, Jinsung Yoon, Chun-Liang Li, Chen-Yu Lee, and Tomas Pfister. Anomaly clustering: Grouping images into coherent clusters of anomaly types. In *Proceedings of the IEEE/CVF Winter Conference on Applications of Computer Vision*, pages 5479–5490, 2023.

Muhammad Tirmazi, Adam Barker, Nan Deng, Md Ehtesam Haque, Zhijing Gene Qin, Steven Hand, Mor Harchol-Balter, and John Wilkes. Borg: the next generation. In *EuroSys'20*, Heraklion, Crete, 2020.

Samantha A Usman, Alexander H Nitz, Ian W Harry, Christopher M Biwer, Duncan A Brown, Miriam Cabero, Collin D Capano, Tito Dal Canton, Thomas Dent, Stephen Fairhurst, Marcel S Kehl, Drew Keppel, Badri Krishnan, Amber Lenon, Andrew Lundgren, Alex B Nielsen, Larne P Pekowsky, Harald P Pfeiffer, Peter R Saulson, Matthew West, and Joshua L Willis. The pycbc search for gravitational waves from compact binary coalescence. *Classical and Quantum Gravity*, 33(21):215004, oct 2016. doi: 10.1088/0264-9381/33/21/215004. URL https://dx.doi.org/10.1088/0264-9381/33/21/215004.

Ashish Vaswani, Noam Shazeer, Niki Parmar, Jakob Uszkoreit, Llion Jones, Aidan N Gomez, Łukasz Kaiser, and Illia Polosukhin. Attention is all you need. *Advances in neural information processing systems*, 30, 2017.

Petar Velivckovic, Guillem Cucurull, Arantxa Casanova, Adriana Romero, Pietro Lio, and Yoshua Bengio. Graph attention networks. In *International conference on learning representations*, 2018.

John Wilkes. More google cluster data. *Google research blog, Nov*, 2011.

Xiaowei Xu, Nurcan Yuruk, Zhidan Feng, and Thomas AJ Schweiger. Scan: a structural clustering algorithm for networks. In *Proceedings of the 13th ACM SIGKDD international conference on Knowledge discovery and data mining*, pages 824–833, 2007.

Zhiming Xu, Xiao Huang, Yue Zhao, Yushun Dong, and Jundong Li. Contrastive attributed network anomaly detection with data augmentation. In *Advances in Knowledge Discovery and Data Mining: 26th Pacific-Asia Conference, PAKDD 2022, Chengdu, China, May 16–19, 2022, Proceedings, Part II*, pages 444–457. Springer, 2022.

Xu Yuan, Na Zhou, Shuo Yu, Huafei Huang, Zhikui Chen, and Feng Xia. Higher-order structure based anomaly detection on attributed networks. In *2021 IEEE International Conference on Big Data (Big Data)*, pages 2691–2700. IEEE, 2021.

G. Zarza, D. Lugones, D. Franco, and E. Luque. Fault-tolerant routing for multiple permanent and non-permanent faults in hpc systems. In *Proceedings of the International Conference on Parallel and Distributed Processing Techniques and Applications (PDPTA)*, pages 144–150, Las Vegas, NV, USA, July 2010.

Yue Zhao, Zain Nasrullah, Maciej K Hryniewicki, and Zheng Li. Lscp: Locally selective combination in parallel outlier ensembles. In *Proceedings of the 2019 SIAM International Conference on Data Mining*, pages 585–593. SIAM, 2019a.

Yue Zhao, Zain Nasrullah, and Zheng Li. Pyod: A python toolbox for scalable outlier detection. *Journal of Machine Learning Research*, 20(96):1–7, 2019b. URL http://jmlr.org/papers/v20/19-011.html.

Ziming Zheng, Li Yu, Wei Tang, Zhiling Lan, Rinku Gupta, Narayan Desai, Susan Coghlan, and Daniel Buettner. Co-analysis of ras log and job log on blue gene/p. In *2011 IEEE International Parallel & Distributed Processing Symposium*, pages 840–851, 2011. doi: 10.1109/IPDPS.2011.83.

Appendix

FlowBench code and data repository: `https://github.com/PoSeiDon-Workflows/flowbench`.
We also provide our documentation: `https://poseidon-workflows.github.io/FlowBench/`.

A Workflow Execution Infrastructure
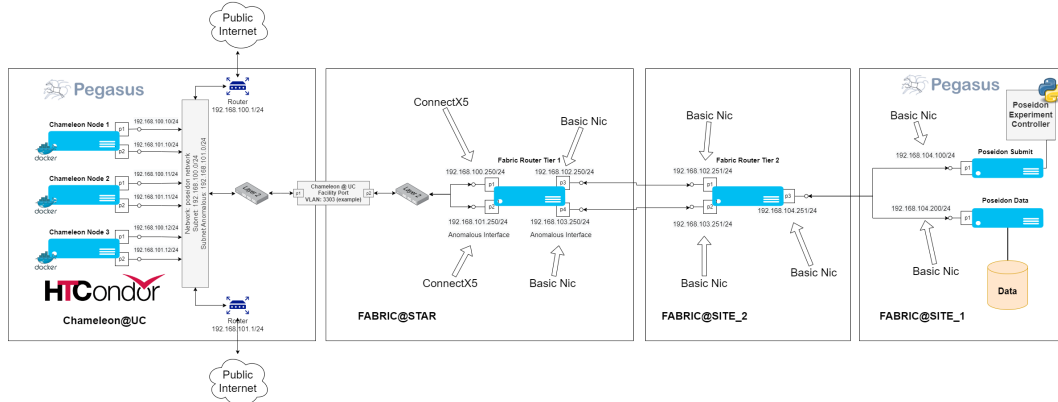
Figure 2: Overview of the execution infrastructure. The deployment spans across the Chameleon Cloud and the FABRIC testbed. Chameleon hosts the workers while FABRIC hosts the networking infrastructure, the workflow submission node and the data storage node. Docker containers are deployed on baremetal nodes and interference (CPU, HDD) is introduced using cgroups. An experimental controller on the workflow submission node orchestrates the anomaly injection, workflow execution triggering and data labeling.

B Workflow Diagrams

Figure 3, 4 and 5 are the workflow diagrams of the 1000 Genome, Montage and Predict Future Sales workflows, respectively.
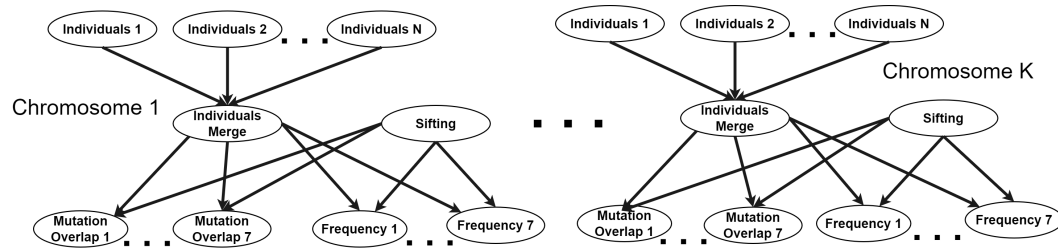
Figure 3: Overview of the 1000Genome sequencing analysis workflow. The workflow creates a branch for each chromosome and each individual task is processing a subset of the Phase 3 data (equally distributed).

C Parsed Features

Table 4 shows the features that are parsed from the Pegasus workflow logs, with the type of each feature and a brief description.

D Benchmark algorithms

Table 5 provide the selected benchmark algorithms and their references. The input X represents using features only, while A, X represents using both structure and features.
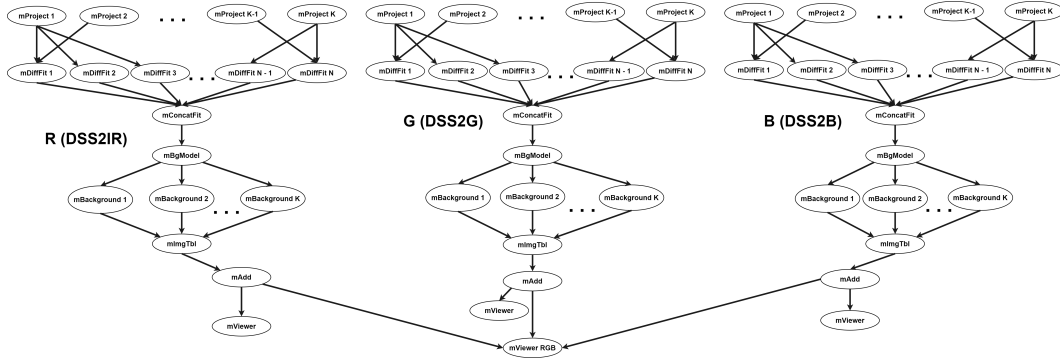
Figure 4: Overview of the Montage workflow. In this case, the workflow uses images captured by the Digitized Sky Survey (DSS) [Association of Universities for Research in Astronomy, 1994] and creates a branch for each band that is requested to be processed during the workflow generation. The size of the first level of each branch depends on the size of the section of the sky to be analyzed, while the second level on the number of overlapping images stored in the archive.

Table 4: Parsed Dataset Features.

Field	Data Type	Description
node_id	string	Exec. DAG Node ID
anomaly_type	string	Anomaly label
type	int	Pegasus job type
is_clustered	int	1 if job clustering enabled else 0
ready	ts	Epoch ts when all dependencies have been met and job can be dispatched
pre_script_start	ts	Epoch ts when the pre-script started executing
pre_script_end	ts	Epoch ts when the pre-script stopped executing
submit	ts	Epoch ts when the job was submitted to the queue
stage_in_start	ts	Epoch ts when the data stage in started
stage_in_end	ts	Epoch ts when the data stage in ended
stage_in_effective_bytes_per_sec	float	Bytes written per second (input data)
execute_start	ts	Epoch ts when the execution starts
execute_end	ts	Epoch ts when the execution ends
stage_out_start	ts	Epoch ts when the data stage out started
stage_out_end	ts	Epoch ts when the data stage out ended
stage_out_effective_bytes_per_sec	float	Bytes written per second (output data)
post_script_start	ts	Epoch ts when the post-script started executing
post_script_end	ts	Epoch ts when the post-script ended executing
wms_delay	float	Composite field estimating the delay introduced by the WMS while preparing the job for submission
pre_script_delay	float	Composite field estimating the delay introduced by the pre-script
queue_delay	float	Composite field estimating the time spent in the queue
runtime	float	Total runtime of the job, based on execute start and end
post_script_delay	float	Composite field estimating the delay introduced by the post-script
stage_in_delay	float	Total time spend staging in data, based on stage in start and end
stage_in_bytes	float	Total bytes staged in
stage_out_delay	float	Total time spend staging out data, based on stage out start and end
stage_out_bytes	float	Total bytes staged out
kickstart_user	string	Name of the user submitted the job
kickstart_site	string	Name of the execution site
kickstart_hostname	string	Hostname of the worker node the job executed on
kickstart_transformations	string	Mapping of the executable locations
kickstart_executables	string	Names of the invoked executables
kickstart_executables_argv	string	Command line arguments used to invoke the executables
kickstart_executables_cpu_time	float	Total cpu time
kickstart_status	int	The status of the job as marked by Pegasus Kickstart
kickstart_executables_exitcode	int	The exitcode of the invoked executable(s)
kickstart_online_iowait	float	Time spent on waiting for io (seconds)
kickstart_online_bytes_read	float	Total bytes read from disk (bytes)
kickstart_online_bytes_written	float	Total bytes written to disk (bytes)
kickstart_online_read_system_calls	float	Number of read system calls
kickstart_online_write_system_calls	float	Number of write system calls
kickstart_online_utime	float	Time spent on user space
kickstart_online_stime	float	Time spent on kernel space
kickstart_online_bytes_read_per_second	float	Bytes read per second (effective)
kickstart_online_bytes_written_per_second	float	Bytes written per second (effective)

E   Data processing

Followed by Table 4, we further processed the parsed data into a dataset in PyTorch-Geometric (PyG) format [Fey and Lenssen, 2019] for the graph-based algorithms. The PyG format is a standard format for graph data in deep learning, which is widely used in the graph neural network (GNN) community. The PyG format is a tuple of $(\mathbf{X}, \mathbf{A}, \mathbf{y})$, where $\mathbf{X}$ is the feature matrix, $\mathbf{A}$ is the adjacency matrix, and $\mathbf{y}$ is the label vector. First, for the features with integers/strings as categories, we processed them into one-hot encoding, and then concatenate them into a feature vector $\mathbf{X}$. Notice that there are multiple features with timestamps, we shifted the timestamp to the same starting point (i.e., the first timestamp
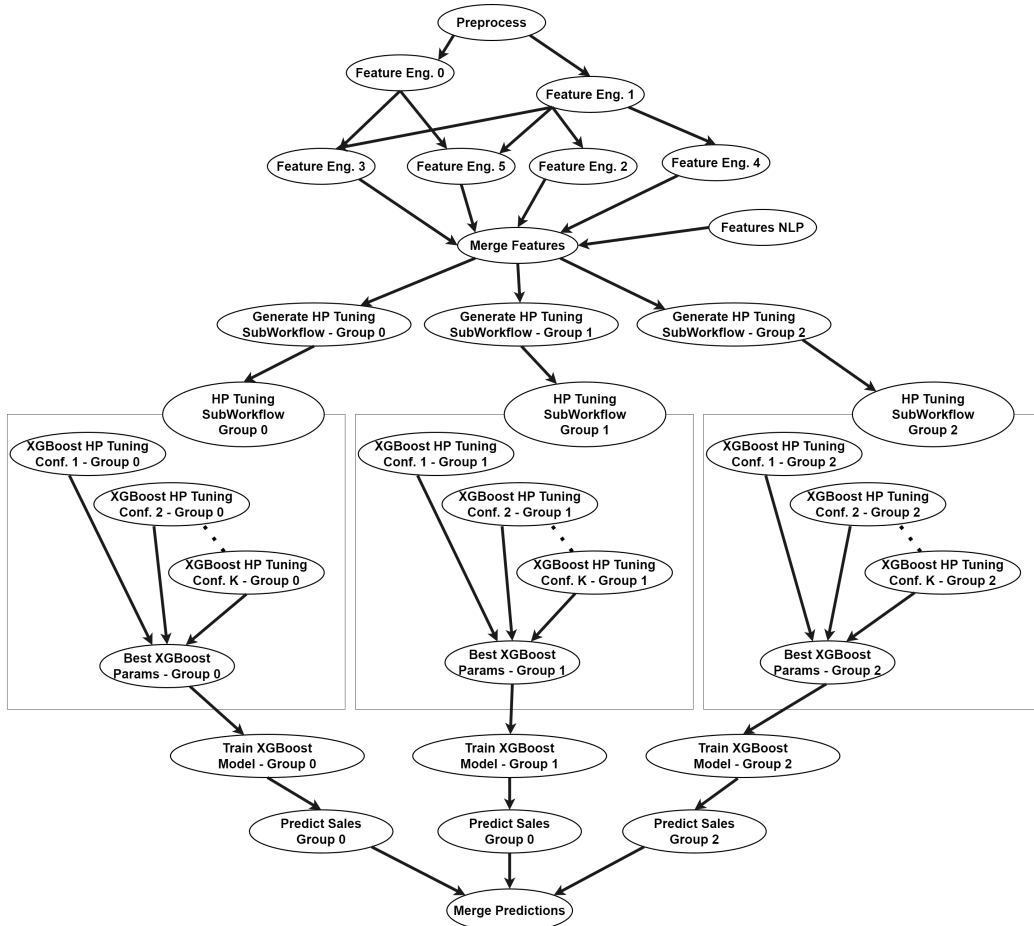
Figure 5: Overview of the Predict Future Sales workflow. The workflow splits the data into 3 item categories and trains 3 XGBoost models that are later combined, using an ensemble technique. It contains 3 hyperparameter tuning subworkfows, that test different sets of features and picks the best performing one. The number of HPO tasks is configurable and depends on the number of combinations that will be tested.

in the dataset), which allows us to measure the behavior of each individual job independently. Moreover, we normalized job feature column-wise, in which we use min-max normalization such that normalized features are in the range $[0, 1]$. Second, for the structural information, we convert the dependencies as directed edges between nodes, and furthermore, we convert the directed acyclic graphs into undirected graphs as $\mathbf{A}$. Finally, we use the label vector $\mathbf{y}$ to indicate job anomalies, where 1 indicates anomalous jobs and 0 indicates normal jobs. For the experiment in the paper, we split the dataset into training, validation, and test set with a ratio 0.6, 0.2, and 0.2, and use the dataloader to load the dataset in mini-batch for training. All the steps are built into a pipeline as the transform class in PyG, which allows us to easily process the dataset into PyG format.

F   Detailed benchmark settings for algorithms

Following in Table 5, we provide the detailed settings for each algorithm used in the benchmark. Notice that we use the default settings for all the algorithms, and we do not tune the hyperparameters for each algorithm. For the hyperparameters that are not listed below, we use the default settings in the implementation of each algorithm from PyOD and PyGOD.

- **ABOD**. N/A.
- **CBLOF**. Check estimator: False.
- **FB**. Number of neighbors: 35.
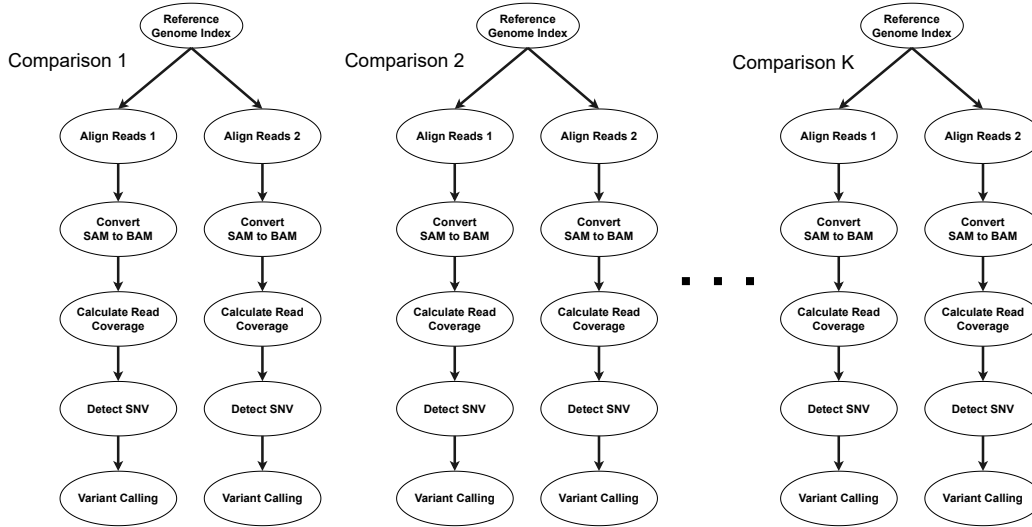
Figure 6: Overview of the Variant Calling Workflow. The workflow compares a DNA sequence to a reference genome and performs multiple comparisons in parallel.
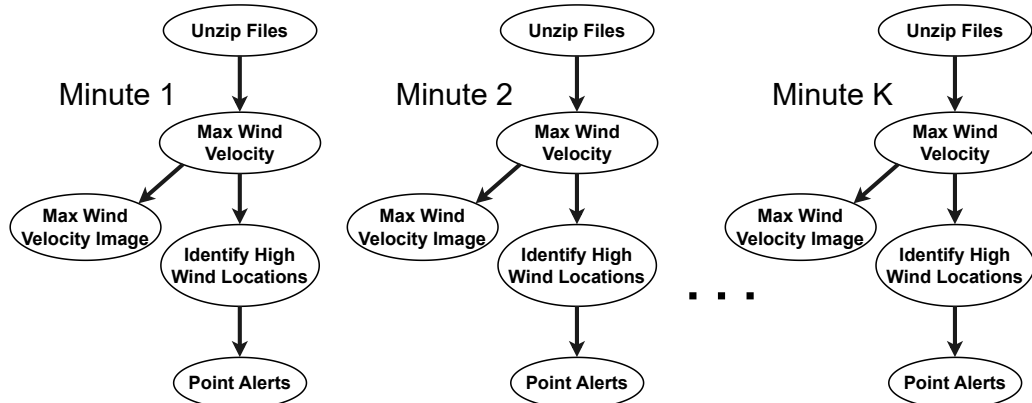

Figure 7: Overview of the CASA Wind Speed Workflow. The wind speed workflows calculates the max wind velocity in increments of one minute. Multiple minutes are calculated in parallel.

- **HBOS**. N/A.
- **IF**. N/A.
- **KNN**. N/A.
- **AKNN**. Aggregation method: average.
- **LOF**. Number of neighbors: 35.
- **MCD**. N/A.
- **OCSVM**. N/A.
- **PCA**. N/A.
- **LSCP**. Detector list with a set of LOF models on a number of neighbors: 5, 10, 15, 20, 25, 30, 35, 40, 45, 50.
- **INNE**. Max samples: 2.
- **GMM**. N/A.
- **KDE**. N/A.
- **LMDD**. N/A.
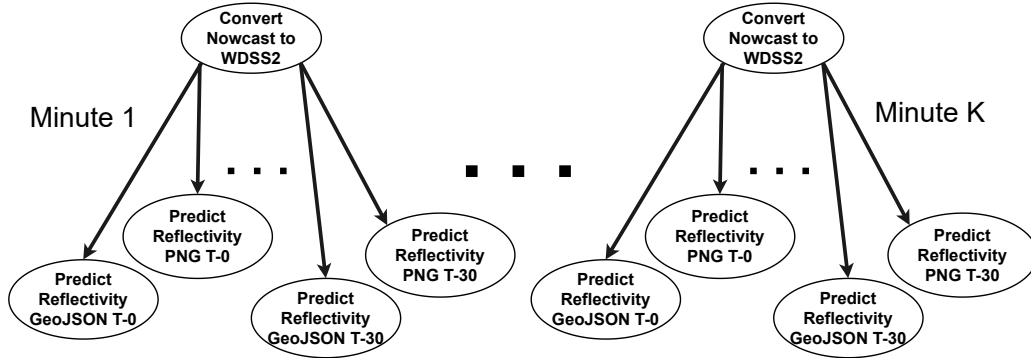
Figure 8: Overview of the CASA Nowcast Workflow. The nowcast workflow forecasts the nowcast events for the next thirty minutes. The forecats are based on one minute radar data. Multiple minutes of data are calculated in parallel.
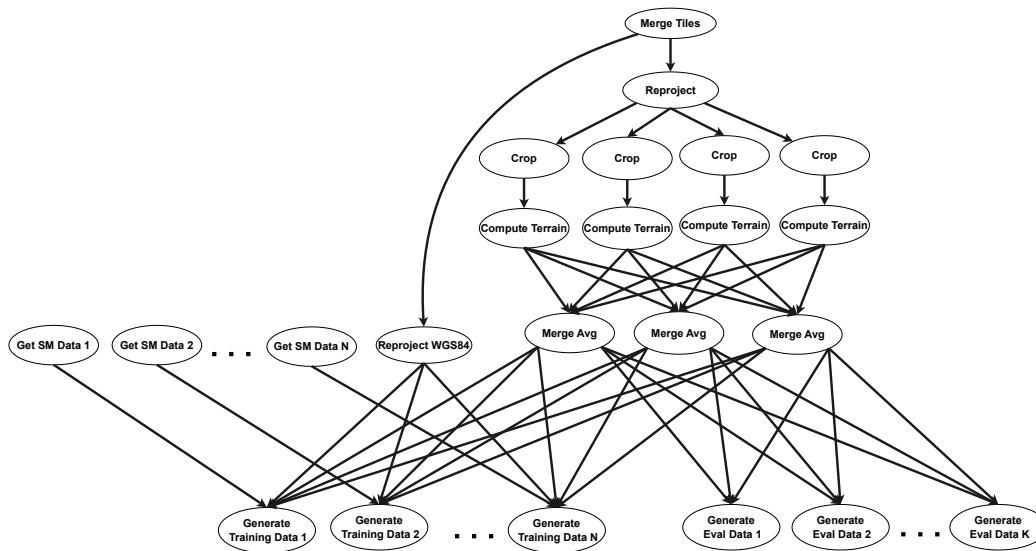

Figure 9: Overview of the Soil Moisture Spatial Inference Engine Workflow - Data Preparation. The workflow fetches and process environmental data for a specified region using USGS data.

- **MLPAE**. Hidden dimension: 64, batch size: 64 learning rate: 1e-3, weight decay: 1e-5, dropout: 0.5, epochs: 200.

- **SCAN**. $\epsilon = 0.5$, $\mu = 5$.

- **Radar**. Learning rate: 1e-3.

- **Anomalous**. Learning rate: 1e-3.

- **GCN**. Hidden dimension: 64, batch size: 64, learning rate: 1e-3, weight decay: 0, dropout: 0.5, epochs: 200.

- **GraphSAGE**. Hidden dimension: 64, batch size: 64, learning rate: 1e-3, weight decay: 0, dropout: 0.5, epochs: 200.

- **GCNAE**. Hidden dimension: 64, batch size: 64 learning rate: 1e-3, weight decay: 1e-5, dropout: 0.5, epochs: 200.

- **Dominant**. Hidden dimension: 64, batch size: 64 learning rate: 1e-3, weight decay: 1e-5, dropout: 0.5, epochs: 200.

- **DONE**. Hidden dimension: 64, batch size: 64 learning rate: 1e-3, weight decay: 1e-5, dropout: 0.5, epochs: 200.
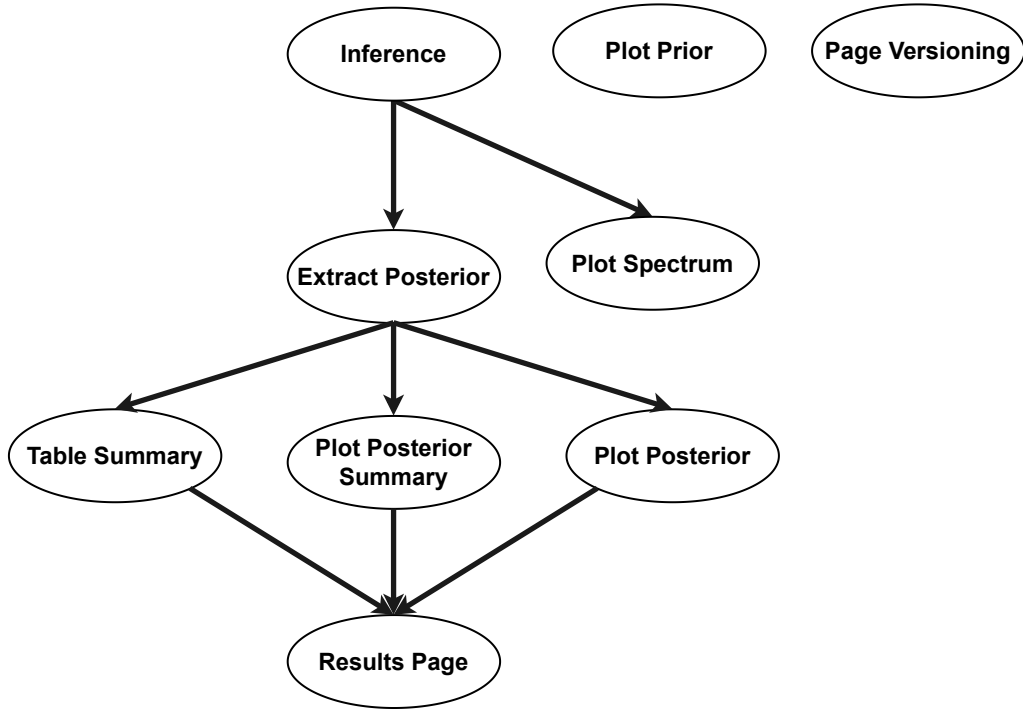
Figure 10: Overview of the PyCBC Inference Workflow. The inference workflow performs parameter estimation on gravitational wave signals using prior knowledge and Bayesian approaches.

- **ADONE**. Hidden dimension: 64, batch size: 64 learning rate: 1e-3, weight decay: 1e-5, dropout: 0.5, epochs: 200.
- **AnomalyDAE**. Hidden dimension: 64, batch size: 64 learning rate: 1e-3, weight decay: 1e-5, dropout: 0.5, epochs: 200, $\alpha = 0.5$, $\theta = 10$, $\eta = 5$.
- **GAAN**. Hidden dimension: 64, batch size: 64 learning rate: 1e-3, weight decay: 1e-5, dropout: 0.5, epochs: 200.
- **GUIDE**. Feature hidden dimension: 64, structure hidden dimension: 5, batch size: 64 learning rate: 1e-3, weight decay: 1e-5, dropout: 0.5, epochs: 200.
- **CONAD**. Hidden dimension: 64, batch size: 64 learning rate: 1e-3, weight decay: 1e-5, dropout: 0.5, epochs: 200.
- **DeepSAD**. Batch size: 128, learning rate: 1e-3, epochs: 50.
- **REPEN**. Hidden dimension: 20, batch size: 256, epochs: 1000.
- **PReNet**. Batch size: 512, learning rate: 1e-3, epochs: 10.

G   Generalization

We are going to discuss generalization based on four points, 1) the type of applications, 2) the extensibility and reproducibility of the data collection 3) the type of injected anomalies and system anomalies, 4) problems involving DAGs.

- **Type of Applications:** In our submission we presented 3 workflow applications that are described using an open-source workflow management tool and they are representative of the High Throughput Computing (HTC) workloads observed in the community. In previous work researchers have used similar workflows to provide a characterization of the scientific workflows seen in the wild [Juve et al., 2013],[Krawczuk et al., 2021]. We selected these workflow applications for the size and complexity of their DAGs (Figure 3, Figure 4, Figure 5), the ability to acquire real execution traces within a reasonable
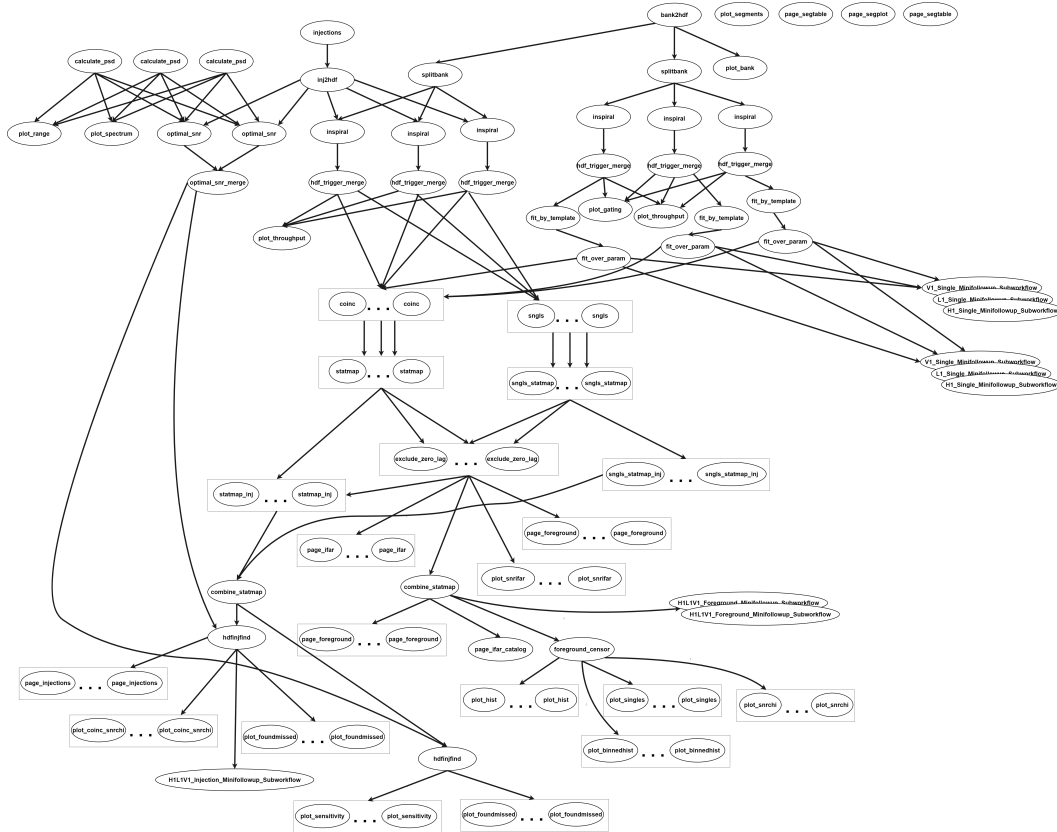
Figure 11: Overview of the PyCBC Search Workflow. The search workflow sifts through data to identify gravitational waves. It contains nine subworkflows for followup studies.
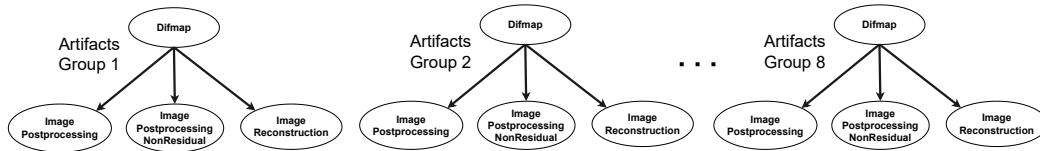

Figure 12: Overview of the EHT Difmap Workflow. The workflow performs image reconstruction by employing iterative convolution with difference mapping.

time for each workflow run and because they are addressing real world problems. By using the binaries executed in each node of the workflow we are not claiming that we can transfer learning directly to other applications and execution systems. Since each binary can be executing different instructions and can be compiled with different optimizations in mind (e.g., infiniband drivers, gpu accelerators) [Phillips et al., 2020],[Kenny et al., 2020]. Additionally, hardware differences among execution environments can lead to different node level performance, overall workflow performance and potentially different results. The majority of the workflow management systems model their workflows as DAGs [Ferreira da Silva et al., 2017],[Mitchell et al., 2019], with dependencies among jobs, creating parent and children relationships, and this dataset captures resource statistics and the behavior of the workflow, tightly coupled with each workflow step. Most datasets that currently exist do not offer this information between application and resources, because they are observing the behavior of the system, instead of the behavior of the application, or because of privacy and security policies.

- **Data Collection**: To generate this dataset, we used resources widely available to the educational community. We used the Chameleon testbed [Keahey et al., 2020] to create our computational infrastructure. And we used publicly available workflows described
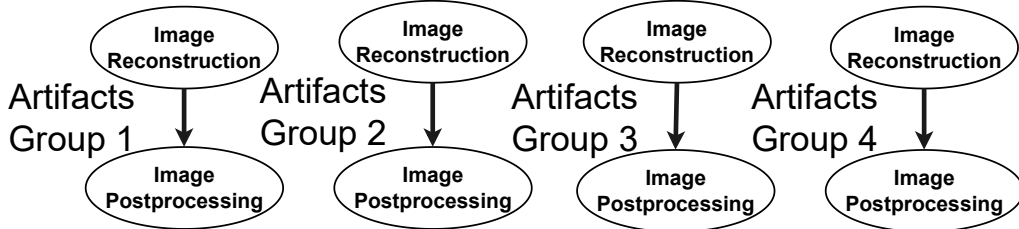
Figure 13: Overview of the EHT Imaging Workflow. The workflow performs image reconstruction using the regularized maximum likelihood (RLM) approach.
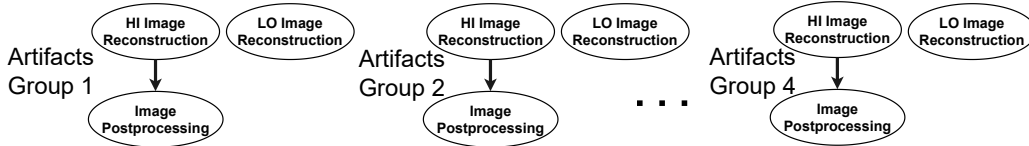

Figure 14: Overview of the EHT Smili Workflow. The workflow uses the Sparse Modeling Imaging Library for Interferometry (SMILI) to incorporate pre-calibrated datasets and perform image reconstruction using the RML approach.

using the Pegasus Workflow Management System [Deelman et al., 2019] and tools that are distributed with it [Papadimitriou et al., 2021]. As a result, if one wants to replicate, extend, or incorporate the monitoring and collection into their workflows it's possible. Additionally, we are planning to share our recipes and code for our experimental harness for anybody that might be interested in using it.

- **Injected Anomalies**: In our work we define anomalies as system slowdowns and not hard failures. More specifically with the CPU anomaly we aim to demonstrate a CPU slowdown due to co-location of tasks on the same host, competing for cpu cycles. We introduce this anomaly via cgroups, restricting our binaries to use only a certain number of cores available to the host. For example when a host has 4 cores and we take away 2 cores, we label this anomaly setting as "CPU_2", in order to mimic the behavior of tasks that have been mapped to the host and are taking 100% of the cpu time on the takeaway cores. This can be caused by misconfiguration or even by poor queue priority choices by the user. Similarly with the HDD anomaly we aim to demonstrate filesystem slowdown due to IO overload or filesystem health status (e.g., filesystem repair). We apply the HDD anomaly using cgroup limits and we limit the worker hosts average read and average write speeds. For example, with the HDD_10 label, we limit the read to 20MB/s and write to 10MB/s. The type of injected anomalies aim to mimic slow downs observed in production systems. For example, at National Energy Research Scientific Computing Center (NERSC) during the execution of the XFEL workflow they discovered a slow down on the shared filesystem, that was delaying or stalling the execution of the tasks [Blaschke et al., 2021].

- **Generalization of DAG datasets**. Not only in the domain of computational workflows but also in other domains, DAGs are widely used to model the dependencies among tasks. For instance, DAGs can be used in social network analysis to model the relationships between individuals, organizations, or communities. In this domain, DAGs can help identify influential individuals or clusters, detect communities, and analyze the spread of information or behaviors. In biology, DAGs can represent gene regulatory networks, where nodes represent genes and edges represent regulatory interactions between them. This allows researchers to study the behavior of genetic systems and identify potential drug targets. In traffic management, DAGs can model traffic flow and help optimize traffic signal control, routing, and traffic assignment. In finance, DAGs can represent relationships between financial instruments, such as stocks, bonds, and currencies, allowing for portfolio optimization and risk analysis. These examples demonstrate the versatility and generalization of DAGs in various domains, making them a valuable tool for understanding and analyzing complex systems.
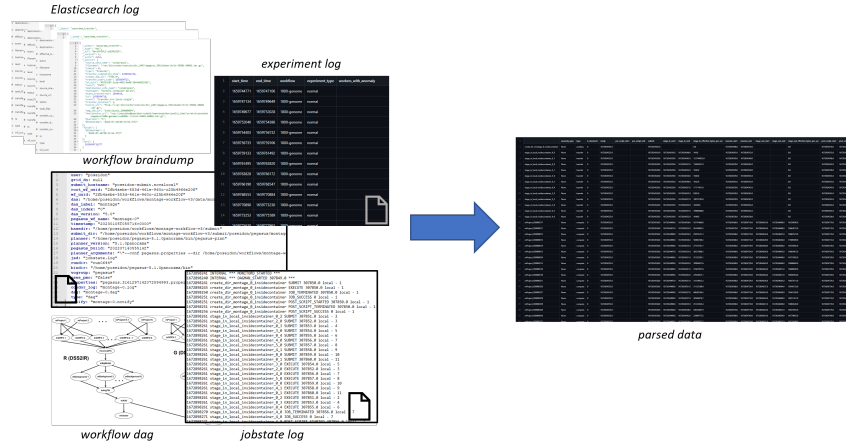
Figure 15: Converting the raw data to the parsed CSV data

H   Other Open Datasets

There are other open datasets that in the past, they have been used to analyze and predict system failures[Oliner and Stearley, 2007],[Zarza et al., 2010],[Zheng et al., 2011], and improve scheduling algorithms and cluster health [Wilkes, 2011],[Tirmazi et al., 2020]. However, these datasets are not suitable for modeling and predicting workflow application performance since they are connections between the workflow application DAGs and the system usage, which we offer in our dataset. A dataset that observes the behavior of the workflow from the application perspective can be found in WfCommons [Coleman et al., 2022], but there are only 180 traces total that exist in the dataset, without any training labels, making the use of these data insufficient for training ML models.

I   Supplementary Benchmarks

We include the complementary benchmark methods here, including semi-supervised (DeepSAD, PReNet) methods provided from ADBench [Han et al., 2022]. To expand Table 2 and 3, we report the additional results in Table 6, which reports the mean accuracy scores across 5 different runs, even though the unsupervised methods do not require labels for training. Some key observations that can be made from the table:

- The supervised and semi-supervised models generally outperform the unsupervised PyOD and PyGOD models.

- The SFT-LLM models (BERT and RoBERTa-large) also perform well, often among the top models for each workflow. Interesting, with a relative model size of 110 M in BERT and 355 M parameters in RoBERTa-large, and parameter efficient training LoRA, is able to achieve competitive performance, showing the training time in Table 3.

- There are some cases where certain models fail to complete the task, indicated by "TLE" (Time Limit Exceeded) or "OOM" (Out Of Memory). This is due to the complexity of the model processing the graph, especially for the larger workflows and more runs in datasets. Even with advanced hardware accelerators, e.g., NVIDIA A100 in our experiments, the model may still fail to complete the task. This is a common issue in graph-based deep learning models, particularly when processing large graphs and their entire structure.

- The performance of the models varies across the different workflows, highlighting the importance of evaluating on multiple real-world datasets.

The table provides a comprehensive comparison of the different anomaly detection models, allowing researchers to evaluate their performance across a wide range of datasets and identify the most suitable approaches for their specific use cases. In addition, due to the most accessible and widely used models from PyOD, we also present the results evaluated with top K precision scores with

Table 5: Selected algorithms for anomaly detection. The input X represents using features only, while A, X represents using both structure and features.

Algorithm	Reference	Input Data	ML Supervision	Backbone
DT	Quinlan [1986]	X	Supervised	Decision Tree
RF	Breiman [2001]	X	Supervised	Random Forest
MLP	Rumelhart et al. [1986]	X	Supervised	MLP
GCN	Kipf and Welling [2017]	A, X	Supervised	GNN
GraphSAGE	Hamilton et al. [2017]	A, X	Supervised	GNN
FTTransformer	Gorishniy et al. [2021]	X	Supervised	Transformer
LLMs (SFT)	Devlin et al. [2018]	X (text)	Supervised	Transformer
GANomaly	Akcay et al. [2019]	X	Semi-supervised	GAN
DeepSAD	Ruff et al. [2019]	X	Semi-supervised	Deep one-class
REPEN	Pang et al. [2019]	X	Semi-supervised	Neighbors
PReNet	Ren et al. [2019]	X	Semi-supervised	Neighbors
ABOD	Kriegel et al. [2008]	X	Unsupervised	Probabilistic
CBLOF	He et al. [2003]	X	Unsupervised	Neighbors
FB	Lazarevic and Kumar [2005]	X	Unsupervised	Ensembles
HBOS	Goldstein and Dengel [2012]	X	Unsupervised	Neighbors
IF	Liu et al. [2008]	X	Unsupervised	Ensembles
KNN	Ramaswamy et al. [2000]	X	Unsupervised	Neighbors
AKNN	Angiulli and Pizzuti [2002]	X	Unsupervised	Neighbors
LOF	Breunig et al. [2000]	X	Unsupervised	Neighbors
MCD	Hardin and Rocke [2004]	X	Unsupervised	Linear
OCSVM	Schölkopf et al. [2001]	X	Unsupervised	Linear
PCA	Shyu et al. [2003]	X	Unsupervised	Decomposition
LSCP	Zhao et al. [2019a]	X	Unsupervised	Ensembles
INNE	Bandaragoda et al. [2018]	X	Unsupervised	Ensembles
GMM	Rasmussen [1999]	X	Unsupervised	Mixture
KDE	Latecki et al. [2007]	X	Unsupervised	Probabilistic
LMDD	Arning et al. [1996]	X	Unsupervised	Linear
MLPAE	Sakurada and Yairi [2014]	X	Unsupervised	MLP, AE
SCAN	Xu et al. [2007]	A, X	Unsupervised	Clustering
Radar	Li et al. [2017]	A, X	Unsupervised	Decomposition
Anomalous	Peng et al. [2018]	A, X	Unsupervised	Decomposition
GCNAE	Kipf and Welling [2016]	A, X	Unsupervised	GNN, Auto-encoder
Dominant	Ding et al. [2019]	A, X	Unsupervised	GNN, Auto-encoder
DONE	Bandyopadhyay et al. [2020]	A, X	Unsupervised	MLP, Auto-encoder
ADONE	Bandyopadhyay et al. [2020]	A, X	Unsupervised	MLP, Auto-encoder
AnomalyDAE	Fan et al. [2020]	A, X	Unsupervised	GNN, Auto-encoder
GAAN	Chen et al. [2020]	A, X	Unsupervised	GAN
GUIDE	Yuan et al. [2021]	A, X	Unsupervised	GNN, Auto-encoder
CONAD	Xu et al. [2022]	A, X	Unsupervised	GNN, Auto-encoder

different models in Figure 17. It allows to compare the performance of the models across different datasets and identify the most effective models for each workflow.

Table 6: Model Comparison - with selected models from different approaches.

workflow	PyOD						PyGOD		Supervised		Semi-supervised		SFT-LLMs	
	GMM	KNN	LMDD	PCA	GAE	DONE	CONAD	AnomalyDAE	GCN	MLP	DeepSAD	PReNet	BERT	RoBERTa-large
1000genome	.660	.691	.673	.626	.643	.655	0.677	.664	.794	.799	.708	.742	.776	.808
casa nowcast full	.768	.774	TLE	.760	.746	OOM	OOM	OOM	.784	.770	.745	.729	.796	.768
casa wind full	.757	.779	.793	.749	.760	OOM	0.749	OOM	.791	.774	.755	.766	.795	.812
eht difmap	.748	.772	TLE	.752	.741	.772	OOM	OOM	.786	.775	.767	.761	.784	.807
eht imaging	.815	.794	.839	.728	.728	.824	0.710	.731	.817	.850	.774	.796	.825	.819
eht smili	.768	.776	.805	.730	.742	.813	0.733	.728	.805	.820	.784	.768	.840	.842
montage	.755	.780	.795	.748	.735	OOM	0.745	.766	.795	.828	.780	.773	.803	.805
predict future sales	.773	.825	.807	.770	.790	OOM	0.801	.825	.814	.839	.802	.826	.861	.813
pycbc inference	.793	.844	TLE	.782	.776	OOM	OOM	OOM	.815	.827	.819	.803	.829	.808
pycbc search	.762	.795	.759	.763	.776	.795	0.783	.783	.809	.800	.778	.750	.825	.790
somospie	.764	.799	TLE	.725	.699	OOM	OOM	OOM	.801	.795	.745	.740	.809	.810
variant calling	.762	.773	TLE	.751	.764	OOM	OOM	OOM	.788	.819	.780	.797	.791	.778
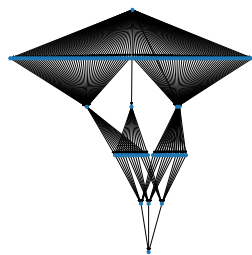
(a) 1000 Genome
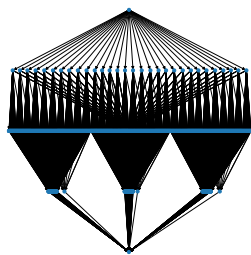
(b) CASA Nowcast
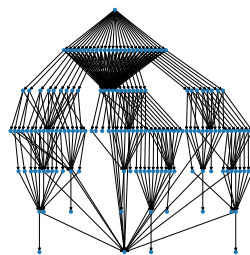
(c) CASA Wind
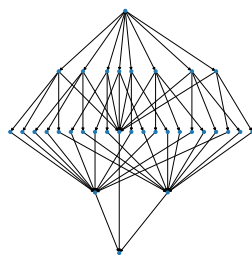
(d) EHT Difmap
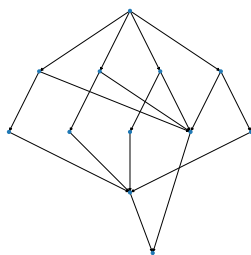
(e) EHT Imaging
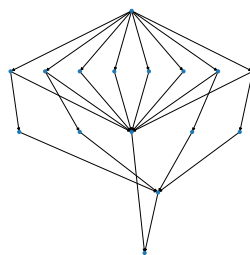
(f) EHT Smili
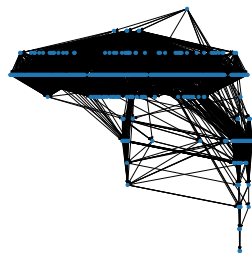
(g) Montage
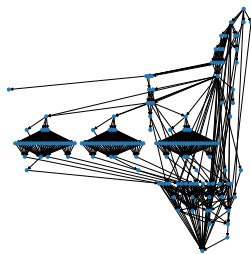
(h) Predict Future Sales
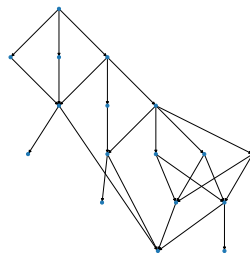
(i) PyCBC Inference
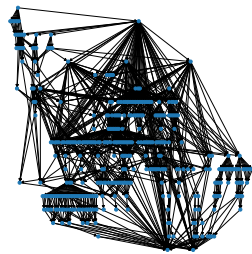
(j) PyCBC Search
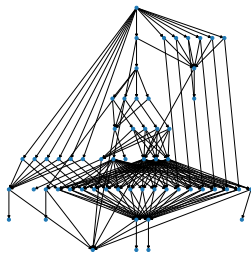
(k) Somospie
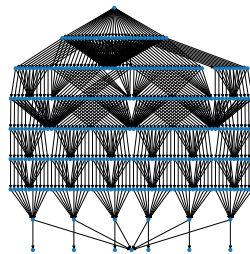
(l) Variant Calling

Figure 16: Workflow visualizations
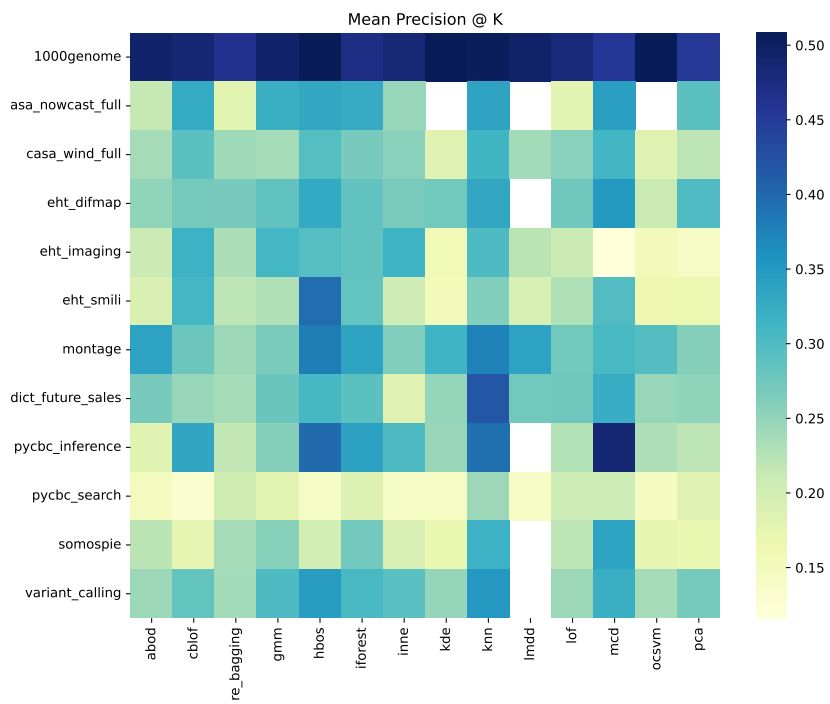
Figure 17: Heatmap of the PyOD algorithms on the benchmark datasets. Reported mean precision score at K.